The Company of
Biologists

RESEARCH ARTICLE

Sphingolipids inhibit endosomal recycling of nutrient transporters by inactivating ARF6

Brendan T. Finicle*, Manuel U. Ramirez*, Gang Liu, Elizabeth M. Selwan, Alison N. McCracken, Jingwen Yu, Yoosun Joo, Jannett Nguyen, Kevin Ou, Saurabh Ghosh Roy, Victor D. Mendoza, Dania Virginia Corrales and Aimee L. Edinger‡

ABSTRACT

Endogenous sphingolipids (ceramide) and related synthetic molecules (FTY720, SH-BC-893) reduce nutrient access by decreasing cell surface expression of a subset of nutrient transporter proteins. Here, we report that these sphingolipids disrupt endocytic recycling by inactivating the small GTPase ARF6. Consistent with reported roles for ARF6 in maintaining the tubular recycling endosome, MICAL-L1-positive tubules were lost from sphingolipid-treated cells. We propose that ARF6 inactivation may occur downstream of PP2A activation since: (1) sphingolipids that fail to activate PP2A did not reduce ARF6-GTP levels; (2) a structurally unrelated PP2A activator disrupted tubular recycling endosome morphology and transporter localization; and (3) overexpression of a phosphomimetic mutant of the ARF6 GEF GRP1 prevented nutrient transporter loss. ARF6 inhibition alone was not toxic; however, the ARF6 inhibitors SecinH3 and NAV2729 dramatically enhanced the killing of cancer cells by SH-BC-893 without increasing toxicity to peripheral blood mononuclear cells, suggesting that ARF6 inactivation contributes to the anti-neoplastic actions of sphingolipids. Taken together, these studies provide mechanistic insight into how ceramide and sphingolipid-like molecules limit nutrient access and suppress tumor cell growth and survival.

KEY WORDS: Nutrient transporters, ARF6, Endosomal recycling, Sphingolipids, GRP1

INTRODUCTION

Sphingolipids induce an evolutionarily conserved adaptive quiescence program in stressed cells that depends on the downregulation of nutrient transporters. Phytosphingosine starves heat-stressed yeast into growth arrest by triggering the internalization of several nutrient permeases, including the tryptophan transporters TAT1 and TAT2, the uracil transporter FUR4 and the general amino acid permease GAP1 (Bultynck et al., 2006; Chung et al., 2001; Dickson et al., 1997; Skrzypek et al., 1998; Welsch et al., 2004). In mammalian cells, ceramide produced in response to a variety of stresses antagonizes growth and proliferation, in part by downregulating nutrient transporter proteins and reducing amino acid and glucose import (Guenther

et al., 2008, 2014; Hannun and Obeid, 2008; Summers et al., 1998). Attributing cellular phenotypes to specific endogenous sphingolipids is complicated by the fact that a large number of enzymes rapidly metabolize sphingolipids into derivatives that can have different, and even opposing, effects on cells (Hannun and Obeid, 2008). Using synthetic, sphingolipid-like molecules can help to overcome this problem. Similar to the endogenous sphingolipids phytosphingosine and ceramide, the FDA-approved sphingolipid drug FTY720 triggers transporter downregulation and induces a starvation-like response in both yeast and mammalian cells (Barthelemy et al., 2017; Romero Rosales et al., 2011; Welsch et al., 2004). FTY720 is a pro-drug, and FTY720 phosphate produced intracellularly is responsible for the therapeutic, immunosuppressive actions via stimulation of sphingosine-1-phosphate (S1P) receptors (Brinkmann et al., 2010). Unphosphorylated FTY720, in contrast, limits tumor cell growth and survival *in vitro* and *in vivo* by activating PP2A and disrupting endocytic trafficking (Kim et al., 2016; Romero Rosales et al., 2011). Unlike FTY720, the conformationally constrained FTY720 analog SH-BC-893 (893) does not activate S1P receptors, even in its phosphorylated form (Chen et al., 2016; Kim et al., 2016; Perryman et al., 2016). However, FTY720 and 893 produce identical disruptions in intracellular trafficking, and their IC50 values are closely matched, suggesting that effects on trafficking, not S1P receptors, are responsible for the anti-cancer activity of FTY720 (Kim et al., 2016; Romero Rosales et al., 2011). FTY720 and 893 disrupt the trafficking of transporters for glucose (GLUT1, also known as SLC2A1), pyruvate, lactate and acetate (MCT1, also known as SLC16A1; MCT4, also known as SLC16A3), glutamine (ASCT2, also known as SLC1A5) and leucine (LAT1, also known as SLC7A5) (Barthelemy et al., 2017; Kim et al., 2016). Downregulation of multiple mammalian nutrient transporters by sphingolipids is consistent with the observation that both phytosphingosine and FTY720 promote internalization of permeases for multiple amino acids (tryptophan, leucine, histidine and proline) and uracil in yeast (Barthelemy et al., 2017; Bultynck et al., 2006; Chung et al., 2000, 2001; Skrzypek et al., 1998). In summary, synthetic molecules like FTY720 and 893 phenocopy the growth suppressive effects of endogenous sphingolipids on endocytic trafficking while minimizing the confounding effects of sphingolipid metabolism.

The molecular mechanism underlying sphingolipid-induced nutrient transporter loss has been dissected in yeast. Phytosphingosine triggers actin-dependent endocytosis of nutrient transporters by inducing TORC2-dependent phosphorylation of the pleckstrin-homology (PH) domain-containing proteins SLM1 and SLM2 and RSP5-dependent ubiquitylation of the transporters (Bultynck et al., 2006; Chung et al., 2000; Daquinag et al., 2007; Fadri et al., 2005). Unfortunately, although sphingolipid-induced

Department of Developmental and Cell Biology, University of California Irvine, Irvine, CA 92697, USA.
*These authors contributed equally to this work

‡Author for correspondence (aedinger@uci.edu)

G.L., 0000-0001-9662-7948; Y.J., 0000-0001-6507-288X; K.O., 0000-0003-4689-8998; S.G., 0000-0002-4766-4408; A.L.E., 0000-0003-4277-4584

1

transporter loss is conserved in mammalian cells, the molecular details are not. We have thus far been unable to detect ubiquitylation of nutrient transporters or a role for the RSP5 homolog NEDD4 in mammalian cells treated with FTY720 or ceramide, and there are no clear mammalian orthologs of the SLM1 or SLM2 proteins that promote actin polarization, eisosome organization and endocytic recycling in yeast (Douglas and Konopka, 2014; Kamble et al., 2011; Olivera-Couto et al., 2011; Walther et al., 2006). However, a DELTA-BLAST search against the human proteome indicates that the PH domains of SLM1 and SLM2 bear homology to the PH domains present in the ARF6 GAP ACAP2 (centaurin β2) and in the cytohesin family of ARF6 GEFs [cytohesin-1, cytohesin-2 (ARNO), cytohesin-3 (GRP1), cytohesin-4]. This similarity is interesting because ARF6 regulates actin dynamics, endocytosis and recycling, the same processes controlled by the SLM proteins (Donaldson and Jackson, 2011; Schweitzer et al., 2011). Sphingolipids have not previously been linked to ARF6 regulation. Rather, the available evidence suggests that sphingolipids downregulate nutrient transporter proteins in mammalian cells by activating the serine and threonine protein phosphatase 2A (PP2A). Ceramide, FTY720 and 893 activate PP2A *in vitro* whereas dihydroceramide, a sphingolipid that does not kill cells, does not (Chalfant et al., 2004; Dobrowsky et al., 1993; Kim et al., 2016). PP2A activation is necessary for sphingolipid-induced nutrient transporter loss, as PP2A inhibition with calyculin A or SV40 small t antigen expression maintains transporters on the cell surface in the presence of ceramide, FTY720 or 893 (Guenther et al., 2008; Kim et al., 2016; Romero Rosales et al., 2011). How PP2A activation triggers transporter loss is not understood. Intriguingly, many of the proteins that are downregulated by sphingolipids are also cargo for the ARF6-dependent, clathrin-independent endocytic trafficking pathway (Eyster et al., 2009; Maldonado-Báez et al., 2013), leading to the hypothesis that PP2A may regulate ARF6-dependent trafficking. Here, we show that the 'tumor suppressor lipid' ceramide and the anti-neoplastic sphingolipid-like small molecules FTY720 and 893 decrease cell surface nutrient transporter levels in mammalian cells by reducing ARF6-GTP levels, dissolving the tubular recycling endosome and disrupting endocytic recycling.

RESULTS

Natural and synthetic sphingolipids trap cell surface nutrient transporters in a recycling compartment

CD98 (4F2hc, SLC3A2) is a chaperone protein for LAT1 (SLC7A5) and xCT (SLC7A11), two amino acid transporter proteins whose overexpression in cancer cells is correlated with poor prognosis (Selwan et al., 2016). FTY720 downregulates CD98 and LAT1 in mammalian cells (Barthelemy et al., 2017; Kim et al., 2016; Romero Rosales et al., 2011). Surface levels of CD98 are readily quantified using flow cytometry while antibodies recognizing the exofacial domains of other nutrient transporters are not generally available, most likely because glycosylation of the extracellular regions of these proteins sterically hinders antibody binding. As expected, the sphingolipids ceramide, sphingosine, FTY720 and 893 downregulated CD98 in mammalian cells (Guenther et al., 2008; Kim et al., 2016; Perryman et al., 2016; Romero Rosales et al., 2011; Fig. 1A,B and Fig. S1). Importantly, bacterial sphingomyelinase, an enzyme that converts plasma membrane sphingomyelin into physiological long-chain ceramides, also reduces cell surface levels of transporters, indicating that natural ceramides, not just more-soluble short-chain analogs, share this activity (Guenther

et al., 2008; Fig. 1A,B). As small molecule and protein inhibitors of PP2A block transporter loss (Guenther et al., 2008; Kim et al., 2016; Romero Rosales et al., 2011), this phenotype is not due to the direct effects of sphingolipids on membranes (Trajkovic et al., 2008).

To begin to dissect the mechanism underlying sphingolipid-induced nutrient transporter loss in mammalian cells, a kinetic study of transporter colocalization with markers for different endocytic compartments was performed. In sphingolipid-treated cells, internalized CD98 did not colocalize with the early endosome marker EEA1 at any time point (Fig. 1C and Fig. S2A,B). Sphingolipids induced colocalization of intracellular CD98 and the trans-Golgi network marker TGN46; however, TGN46 localization was itself altered by sphingolipids (Fig. 1D, Fig. S2C,D and Fig. S3A,B). In control cells, TGN46 was mostly colocalized with GM130 as expected (Fig. S3A). In FTY720-treated cells, some TGN46 still colocalized with GM130, but most TGN46 molecules were redistributed to peripheral, vesicular structures. GM130 localization was not altered, suggesting that the cis-Golgi remained intact. While the steady state localization pattern of TGN46 is predominantly in the trans-Golgi network, TGN46 traffics between the trans-Golgi network and the plasma membrane along tubular endosome intermediates (Ghosh et al., 1998; Maxfield and McGraw, 2004; Prescott et al., 1997). The peripheral punctate distribution of both TGN46 and CD98 in sphingolipid-treated cells (Fig. 1D and Fig. S2C,D) suggested that both were trapped in a recycling intermediate. Consistent with this hypothesis, a subset of internalized transferrin receptor (TfR) colocalized with GLUT1 in sphingolipid-treated cells, most likely in recycling endosomes that receive cargo from both the clathrin-independent endocytosis (CIE) and clathrin-mediated endocytosis (CME) pathways (Fig. 1E and Fig. S4A,B). Sphingolipids also increased co-localization of TGN46 and TfR, again suggesting that recycling pathways are disrupted (Fig. S3B). CD98 partially colocalized with the late endosome/lysosome marker LAMP1 only at late time points (Fig. 1F, Fig. S4C,D) suggesting that nutrient transporters that fail to recycle may eventually be rerouted towards the degradative pathway. In ceramide-treated cells, CD98 was present in the interior of the LAMP1-positive endosomes, suggesting it was present in the limiting membrane of intraluminal vesicles that have budded into the multivesicular body (MVB) prior to lysosomal degradation (Fig. 1F). In 893-treated cells where intraluminal budding is disrupted due to the mislocalization of the lipid kinase PIKfyve and the loss of $PI(3,5)P_2$ from MVB membranes (Kim et al., 2016), CD98 remained associated with the limiting membranes of LAMP1-positive endosomes (Fig. 1F). Taken together, these colocalization studies suggest that natural and synthetic sphingolipids trap endocytosed nutrient transporters in recycling endosomes, but these proteins are eventually sent to the lysosome for degradation when they fail to recycle.

As mentioned above, small-molecule inhibitors of PP2A rescue cells from the trafficking defects induced by sphingolipids, indicating PP2A activation is necessary to produce these phenotypes. Consistent with this model, dihydroceramide, which differs from ceramide by a single unsaturated bond (Fig. S1) and does not activate PP2A (Chalfant et al., 2004; Dobrowsky et al., 1993; Kowluru and Metz, 1997) also did not alter the localization of CD98, TGN46, GLUT1 or the TfR (Fig. S5A,B). An 893 analog, 893-lactam, that lacks a charge on the pyrrolidine nitrogen fails to downregulate nutrient transporter proteins or induce vacuolation, which are both PP2A-dependent phenotypes
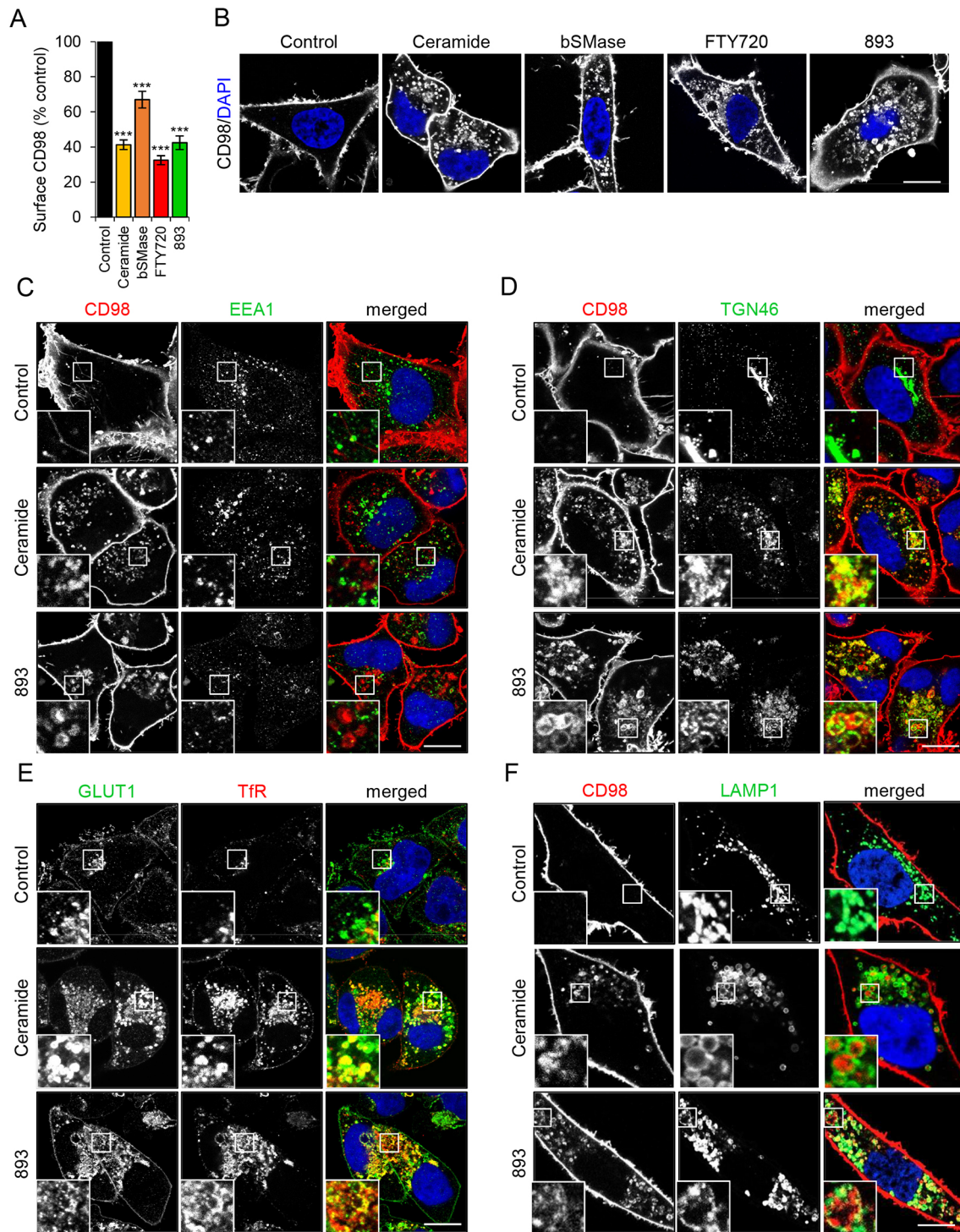
Fig. 1. Natural and synthetic sphingolipids trap plasma membrane nutrient transporters along with recycling cargo. (A) FL5.12 cells were treated with vehicle, C₂-ceramide (50 µM), bacterial sphingomyelinase (bSMase; 100 mU/ml), FTY720 (5 µM) or SH-BC-893 (893, 5 µM) for 3 h then stained for surface CD98. (B) HeLa cells were treated as in A for 12 h then stained for CD98. All images were collected with the same microscope and processed using the same settings. (C-F) HeLa cells were treated with vehicle, C₂-ceramide (50 µM), or 893 (10 µM) for 12 h, then stained for CD98 and EEA1 (C), CD98 and TGN46 (D), GLUT1 and transferrin receptor (TfR) (E), or CD98 and LAMP1 (F). $n \geq 3$ for all panels. Data in A are means±s.e.m. One-way ANOVA was used to compare treated samples with control, ***$P \leq 0.001$. Dunnett's test was used to correct for multiple comparisons. Scale bars: 10 µm. See also Figs S1-S5.

(Fig. S1; Chen et al., 2016; Perryman et al., 2016). Also, 893-lactam did not affect the localization of these recycling proteins (Fig. S5A,B). In summary, a subset of sphingolipids that activate PP2A trap several proteins in what appears to be a recycling compartment.

Sphingolipids increase internalization and block endosomal recycling of nutrient transporters downstream of PP2A activation

The downregulation of nutrient transporter proteins in sphingolipid-treated cells could result from an increased rate of endocytosis, a

decreased rate of endosomal recycling or a combination of the two. Internalization of cell surface transporters in response to sphingolipids was quantified using a flow cytometry-based assay. Briefly, live cells were incubated with unlabeled primary antibody on ice, washed and then shifted to 37°C in the presence or absence of FTY720 for various intervals before staining with fluorochrome-conjugated secondary antibodies on ice. Using this approach, downregulation of molecules that were initially present on the cell surface can be selectively measured. Cell lines that grow in suspension were used for these assays to minimize artifacts that might result from loss of adhesion-dependent signal transduction after trypsinization and to simplify the experimental design. Over the course of the experiment, minimal CD98 was lost from the surface of murine FL5.12 hematopoietic cells in the absence of exogenous sphingolipids, confirming that antibody binding does

not itself trigger CD98 endocytosis (Fig. 2A). Internalization of cell surface CD98 was dramatically enhanced by FTY720 with only 48% of the CD98 molecules that were initially on the surface remaining after 30 min of exposure. Similar results were obtained in human SupB15 leukemia cells. In contrast, FTY720 did not increase transferrin (Tf) internalization in either FL5.12 or SupB15 cells, suggesting that CME is not stimulated by sphingolipids (Fig. 2B). These results suggest that sphingolipids selectively increase the internalization of plasma membrane-localized CD98 but not the TfR.

Endocytic recycling also controls the surface level of plasma membrane proteins. The results in Fig. 2A could have been obtained if CD98 has a high basal internalization rate that was not affected by FTY720 and this sphingolipid selectively blocks recycling. To evaluate whether sphingolipids impede endosomal recycling, a
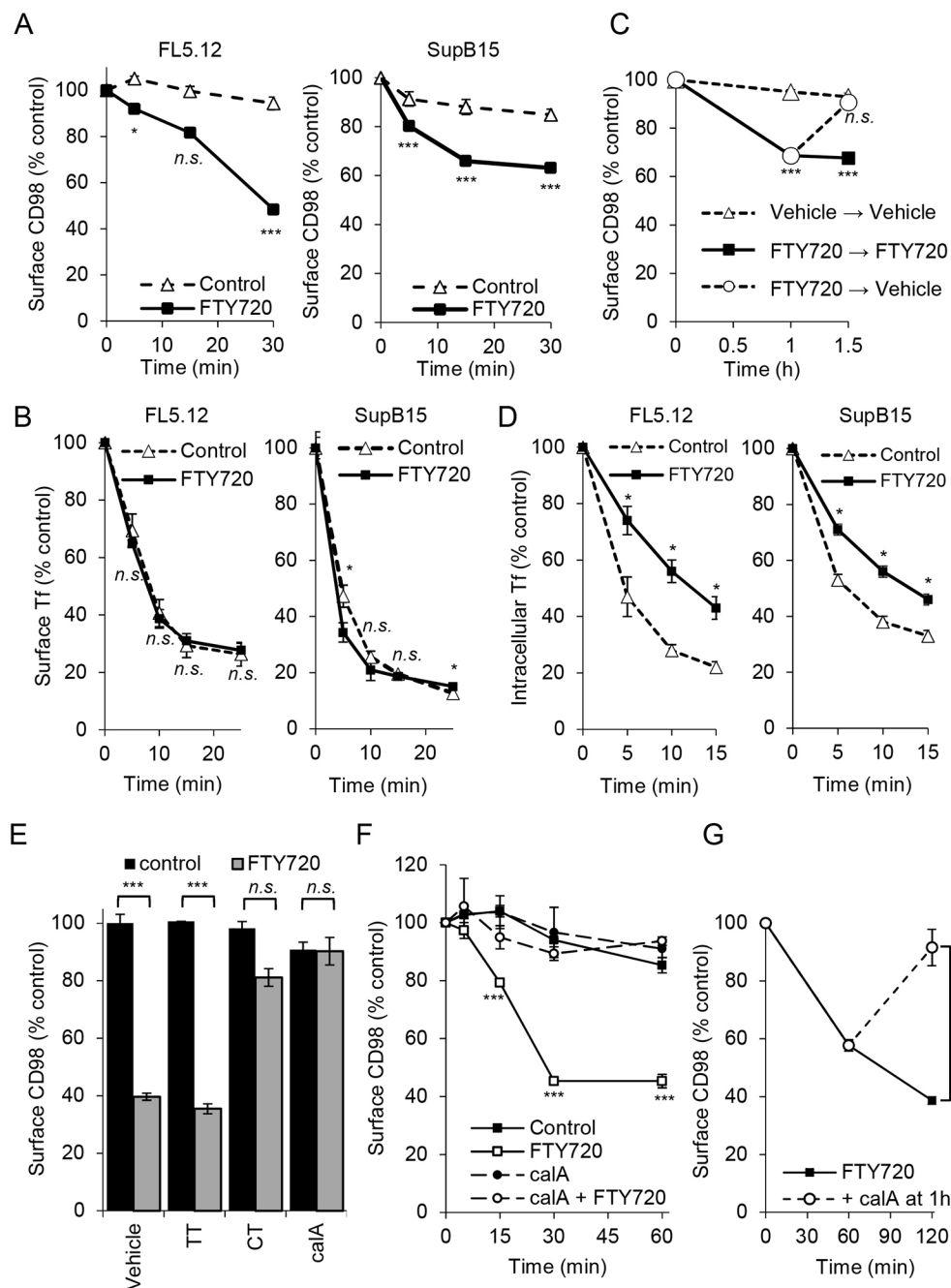

Fig. 2. Sphingolipids inhibit recycling of nutrient transporters in a PP2A-dependent manner. (A) Loss of surface CD98 in FL5.12 and SupB15 cells. Cells were incubated with a primary unconjugated CD98 antibody on ice for 30 min. Cells were then treated with vehicle or FTY720 at 37°C for the indicated times, incubated on ice with secondary antibody for 30 min, and surface CD98 measured by flow cytometry. (B) Transferrin uptake in FL5.12 and SupB15 cells with or without FTY720. (C) CD98 recycling in SupB15 cells. Cells were incubated with primary CD98 antibody as in A, then treated with vehicle or FTY720 for 1 h at which point cells were washed and returned to vehicle- or FTY720-containing medium for 30 min. Surface CD98 levels were then measured by flow cytometry. (D) Tf recycling assay conducted in the presence or absence of FTY720. (E) FL5.12 cells pre-treated (1.5 h) with PP1 inhibitor tautomycin (TT, 200 nM) or PP2A inhibitors cantharidin (CT, 10 μM) or calyculin A (calA, 5 nM) were treated with FTY720 for 1 h and surface CD98 quantified by flow cytometry. (F) Internalization of surface CD98 was measured as in A, cells were pre-treated with calyculin A (5 nM) for 1 h where indicated. (G) Following surface labeling with a primary antibody, FL5.12 cells were treated with FTY720 for 1 h at which point vehicle or calyculin A (10 nM) was added for an additional 1 h. Cells were then stained with secondary antibody and surface CD98 measured using flow cytometry. FTY720 was used at 5 μM. Means±s.e.m. are shown; $n \geq 3$ in all panels. Two-tailed t-test was used to compare sphingolipid-treated time points with vehicle time points. n.s., not significant; $*P \leq 0.05$; $***P \leq 0.001$.

modified version of this flow cytometry assay was utilized. In these recycling studies, surface CD98 was again selectively labeled with primary antibodies, but cells were washed and transferred to FTY720-free medium at 1 h, a time point after CD98 loss had plateaued. As expected, the initial treatment with FTY720 triggered the internalization of about 35% of the cell-surface CD98 in SupB15 cells (Fig. 2A,C). However, washing out FTY720 after 1 h led to the complete restoration of internalized CD98 to the cell surface within 30 min (Fig. 2C). In control samples where FTY720 was replenished after washing, internalized CD98 did not return to the surface. Consistent with the colocalization studies presented in Fig. 1D,E, these results suggest that sphingolipids trap CD98 in a recycling compartment. As TfR was trapped intracellularly along with GLUT1 and TGN46 in sphingolipid-treated cells (Fig. 1E, Fig. S3B and Fig. S4A,B), Tf recycling was also evaluated. Internalized Tf was recycled more slowly in FTY720-treated cells (Fig. 2D). As TfR internalization was not altered by FTY720 (Fig. 2B), sphingolipids may increase the internalization of a subset of clathrin-independent cargo while having a more global negative impact on endocytic recycling.

Sphingolipid-induced nutrient transporter downregulation requires PP2A activation (Guenther et al., 2008; Kim et al., 2016; Romero Rosales et al., 2011). As expected, the PP2A inhibitors calyculin A and cantharidin blocked FTY720-induced nutrient transporter loss (Fig. 2E). Calyculin A and cantharidin inhibit PP1 at ~2-fold and ~10-fold higher concentrations, respectively, than they inhibit PP2A (Swingle et al., 2007). However, the PP1-specific inhibitor tautomycin did not block CD98 loss in response to FTY720 (Fig. 2E). In an internalization assay selectively monitoring cell surface CD98, PP2A inhibition with calyculin A maintained plasma membrane-localized CD98 at initial levels (Fig. 2F). Moreover, the CD98 recycling defect could be attributed to PP2A activation. In recycling assays where cell surface CD98 was labeled and then 1 h was allowed for internalization, calyculin A resulted in the return of internalized CD98 to the cell surface even in the continued presence of FTY720 (Fig. 2G). Taken together, these experiments suggest that PP2A activation by sphingolipids blocks endocytic recycling.

Sphingolipids disrupt the tubular recycling endosome that receives CIE cargo

Several of the nutrient transporter proteins affected by sphingolipids, including CD98, LAT1, GLUT1 and MCT1, are ARF6 cargo proteins that are internalized by CIE and recycled back to the plasma membrane via the tubular recycling endosome (TRE) (Eyster et al., 2009; Maldonado-Báez et al., 2013). The recycling of such cargo from the TRE depends on ARF6-GTP; expressing the dominant-negative ARF6 mutant T27N or knocking down the ARF6 GEF cytohesin-3 (GRP1) ablates endosomal recycling from the TRE (D'Souza-Schorey et al., 1998; Eyster et al., 2009; Li et al., 2012; Maldonado-Báez et al., 2013; Rahajeng et al., 2012; Schweitzer et al., 2011; Zimmermann et al., 2005). The molecular scaffold MICAL-L1 recruits ARF6 to the TRE along with additional proteins involved in membrane tubulation and scission (Cai et al., 2014; Giridharan et al., 2013; Rahajeng et al., 2012; Sharma et al., 2009). Given that the proteins downregulated by sphingolipids are ARF6 cargo that move through the TRE during recycling, we evaluated the effect of sphingolipids on the morphology of this recycling compartment by monitoring MICAL-L1 localization.

HeLa cells are commonly used to study TRE function (Cai et al., 2014; Giridharan et al., 2012, 2013; Rahajeng et al., 2012; Reinecke et al., 2015; Sharma et al., 2009). An extensive TRE is

also present in COS7, COS1, MCF7, dendritic cells and intestinal cells of *Caenorhabditis elegans* (Chen et al., 2014; Grant and Donaldson, 2009; Montesinos et al., 2005; Vidal-Quadras et al., 2011; Walseng et al., 2008; Zimmermann et al., 2005); less elaborate forms of an ARF6-regulated tubular recycling compartment are likely to exist in all mammalian cells. Consistent with the effect of sphingolipids on CD98 internalization and recycling (Fig. 2), both FTY720 and 893 triggered a dramatic relocalization of CD98 to tubular structures within 30 min in HeLa cells (Fig. 3A and not shown). Additional CIE cargo proteins that are downregulated by sphingolipids, GLUT1 and MCT1, also accumulated in tubules in response to FTY720 or 893 (data not shown). To confirm that these tubules represented the TRE, cells were stained for both CD98 and MICAL-L1. Because the antibodies against CD98 and MICAL-L1 were both generated in mice, GFP-tagged MICAL-L1 was expressed to facilitate colocalization studies. As expected, tubules containing CD98 were also positive for MICAL-L1 (Fig. 3B). Moreover, consistent with this structure receiving an enhanced endocytic load, the MICAL-L1-positive TRE expanded upon exposure to 893 (Fig. 3C,D). Following this initial expansion, tubular MICAL-L1 staining was completely lost, shifting to a diffuse, cytoplasmic pattern after 3 h with no decrease in total cellular MICAL-L1 (Fig. 3C-E). Similarly to MICAL-L1, CD98 lost its tubular distribution at 3 h (Fig. 3A) and no longer colocalized with MICAL-L1 at 6 h (Fig. 3F). MICAL-L1 is essential for proper TRE function as it recruits many proteins required for recycling, including ARF6, RAB35, syndapin2, RAB8, RAB10, and EHD1 (Giridharan et al., 2012, 2013; Rahajeng et al., 2012; Sharma et al., 2009). Loss of the molecular scaffold MICAL-L1 suggests that proteins critical for endocytic recycling from the TRE would not be recruited. Indeed, tubular ARF6 and RAB35 staining, and colocalization with MICAL-L1 was eliminated after 6 h of exposure to ceramide or 893 (Fig. S6A,B). These results suggest that the failure to retain MICAL-L1 on the TRE contributes to the disruption in endocytic recycling in sphingolipid-treated cells.

In marked contrast to results obtained with FTY720 and 893 (Fig. 3A-C), ceramide did not induce a tubular MICAL-L1 or CD98 staining pattern at early time points (Fig. 4A,B). While tubular MICAL-L1 persisted until 3 h in cells treated with FTY720 or 893 (Fig. 3C,D), tubular MICAL-L1 localization was lost within 30 min of ceramide addition (Fig. S6A,B). Loss of tubular MICAL-L1 staining in ceramide-exposed cells was not due to degradation as MICAL-L1 total protein levels were not reduced (Fig. 3E). As FTY720, 893 and ceramide induce nutrient transporter loss with similar kinetics and to a similar extent (Fig. 1A-F; Guenther et al., 2008; Kim et al., 2016; Romero Rosales et al., 2011), this discrepancy in their effects on the TRE was unexpected. However, FTY720 and 893 have effects on intracellular trafficking that are not shared with ceramide (Kim et al., 2016). FTY720 and 893 induce profound cytoplasmic vacuolation by mislocalizing the phosphatidyl inositol kinase PIKfyve and its product $PI(3,5)P_2$ to an abnormal compartment, inhibiting activation of the effector protein TRPML1 and the release of Ca^{2+} necessary for lysosomal fusion. Ceramide, in contrast, does not alter PIKfyve localization or inhibit lysosomal fusion reactions. To assess whether the loss of $PI(3,5)P_2$ from the MVB could account for the disparate effects of ceramide and FTY720/893 on MICAL-L1 localization (Fig. 4A), MICAL-L1 localization was evaluated in cells treated with the PIKfyve kinase inhibitor YM201636 alone or in combination with ceramide. Intriguingly, MICAL-L1-positive
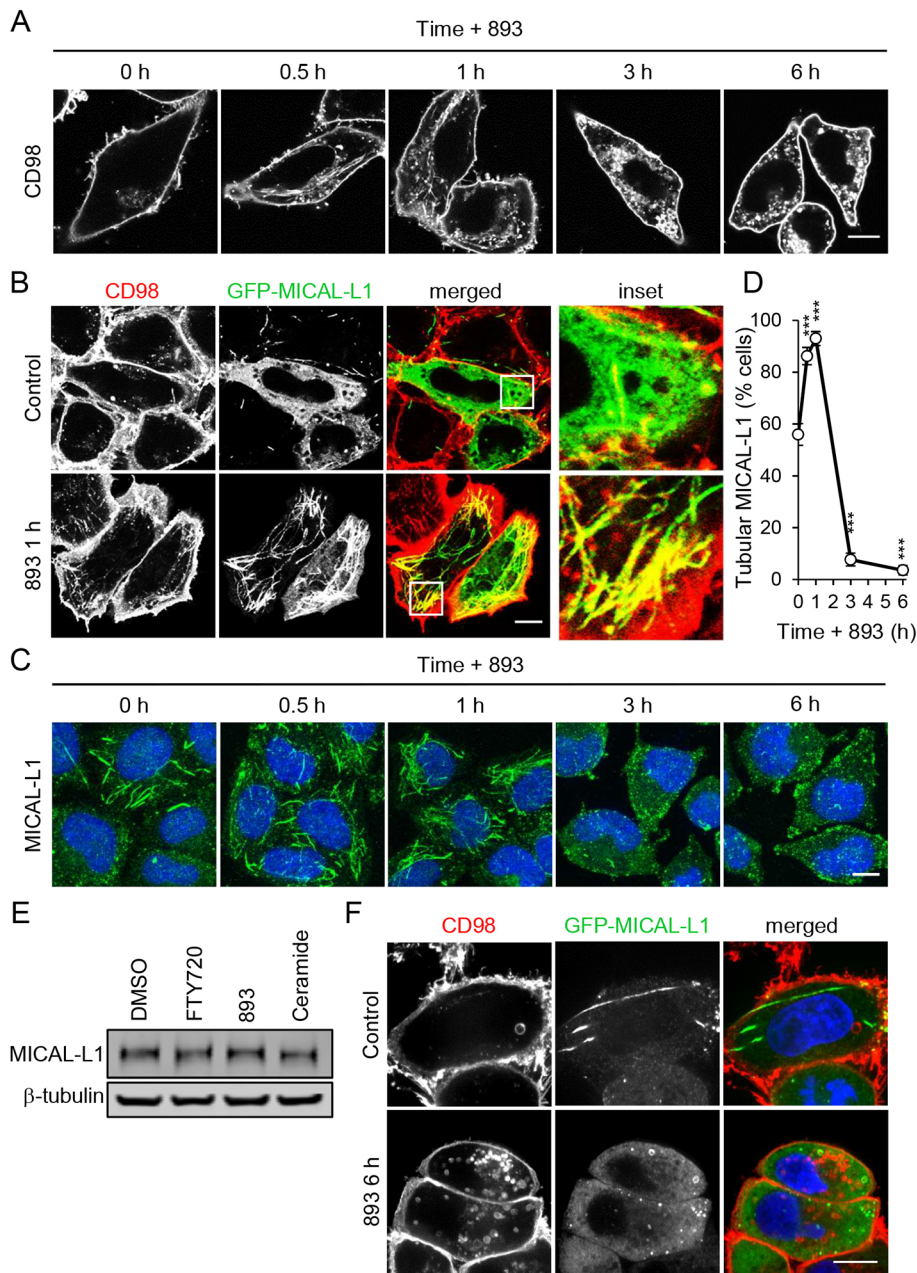
Fig. 3. Sphingolipids send nutrient transporters to the tubular recycling endosome prior to its dissolution. (A) HeLa cells treated with 893 (10 µM) for 0.5, 1, 3 or 6 h were stained for CD98. (B) HeLa cells expressing GFP-MICAL-L1 were treated with 893 (10 µM) for 1 h and stained for CD98. (C) HeLa cells treated as in A but stained for MICAL-L1. (D) Percentage of cells that exhibit tubular MICAL-L1 staining. Means±s.e.m. shown of $n\geq3$. An ordinary one-way ANOVA was used to compare with time zero, ***$P\leq0.001$. Dunnett's test was used to correct for multiple comparisons. (E) Representative blot for HeLa cells treated with FTY720 (10 µM), 893 (10 µM), C_2-ceramide (50 µM) for 6 h, lysed, and blotted for MICAL-L1 and tubulin. (F) HeLa cells expressing GFP-MICAL-L1 treated with 893 (10 µM) for 6 h and stained for CD98. Scale bars: 10 µm.

tubules were longer and more numerous in cells treated with YM201636, a phenotype similar to that seen with FTY720 and 893 at early time points (Fig. 3C,D, Fig. 4A,C and Fig. S6A,B). Whereas about half of the cells normally contain a well-elaborated TRE, nearly 100% of the cells treated with FTY720, 893 or YM201636 contain a TRE structure with extended tubules (Fig. 4A, C,D and Fig. S6A,B). YM201636 did not prevent ceramide-induced dispersion of MICAL-L1, suggesting that FTY720 and 893 may trigger additional trafficking disruptions that affect TRE morphology (Fig. 4D). As YM201636 does not reduce surface nutrient transporter levels as a single agent and does not increase the transporter loss induced by ceramide (Fig. 4C and Kim et al., 2016), it seems unlikely that hypertubulation interferes with recycling or contributes to transporter loss. Rather, the dispersion of MICAL-L1 that is triggered by ceramide immediately or by FTY720 and 893 after 3 h is more likely to be associated with a transporter recycling defect.

Endogenous and synthetic sphingolipids that downregulate nutrient transporters inactivate the ARF6 GTPase

ARF6 activation is required for recycling of a number of cargo proteins that localize to the TRE (D'Souza-Schorey et al., 1998; Donaldson, 2003; Maldonado-Báez et al., 2013). ARF6 is also necessary to maintain the TRE (Rahajeng et al., 2012). Thus, the observed effects of sphingolipids on endocytic recycling and the TRE suggest that sphingolipids might inactivate ARF6. To test this model, ARF6-GTP levels were measured using a published ARF6 effector pull-down assay (Cohen and Donaldson, 2010). The ARF6 inhibitor SecinH3 inactivates the cytohesin family of ARF6 GEFs and reduced ARF6-GTP to about 60% of basal levels; C_2-ceramide, bSMase, FTY720 and 893 decreased ARF6-GTP levels to a similar degree in a dose-responsive and time-dependent manner (Fig. 5A-C). FTY720 inactivated ARF6 in multiple cell types including MDA-MB-231 (human breast cancer), HeLa (human cervical carcinoma), SW620 (human colorectal cancer), PC3
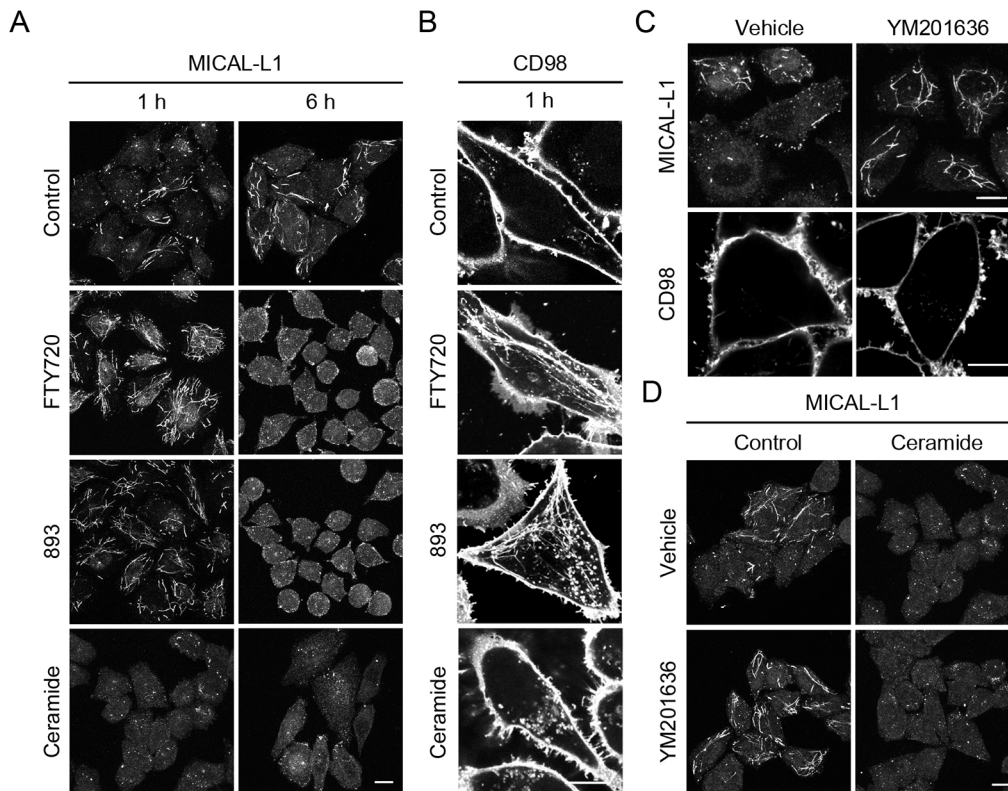
Fig. 4. Hyper-tubulation of the TRE occurs downstream of PIKfyve inhibition. (A) HeLa cells treated with vehicle, FTY720 (10 µM), 893 (10 µM) or C$_2$-ceramide (50 µM) for 1 h or 6 h were stained for MICAL-L1. (B) HeLa cells treated with vehicle, FTY720 (10 µM), 893 (10 µM) or C$_2$-ceramide (50 µM) for 1 h and stained for CD98. (C) HeLa cells treated with PIKfyve inhibitor YM201636 (800 nM) for 1 h and stained for MICAL-L1 or CD98. (D) HeLa cells treated with C$_2$-ceramide (50 µM) or YM201636 (800 nM) alone or in combination for 1 h were stained for MICAL-L1. Scale bars: 10 µm.

(human prostate cancer) and SupB15 (human acute lymphoblastic leukemia) cells (Fig. 5D). Sphingolipids induce nutrient transporter loss in all of these cell types (Guenther et al., 2008; Kim et al., 2016; Romero Rosales et al., 2011). Moreover, sphingolipids that do not downregulate CD98 failed to inactivate ARF6. C$_2$-dihydroceramide did not trigger CD98 downregulation, TGN46 mislocalization, GLUT1 and TfR colocalization, or dissolution of MICAL-L1-positive TRE (Fig. 5E and Fig. S5A-C). C$_2$-dihydroceramide also failed to kill cells (Fig. 5F). Consistent with the expectation that loss of MICAL-L1 on the TRE and mislocalization of recycling cargo TGN46 and TfR is due to ARF6 inactivation, dihydroceramide failed to reduce ARF6-GTP levels (Fig. 5G). Similar results were obtained with the inactive analog 893-lactam (Fig. S5A-D). As C$_2$-dihydroceramide also fails to activate PP2A *in vitro* (Chalfant et al., 2004; Kim et al., 2016), these results are consistent with placement of ARF6 inactivation downstream of PP2A activation. Also consistent with this model, a structurally unrelated small-molecule activator of PP2A, perphenazine (PPZ), was sufficient to trigger mislocalization of CD98 and TGN46 and to eliminate tubular MICAL-L1 staining (Fig. S7A,B). As YM201636 did not alter ARF6-GTP levels or disrupt ARF6 recruitment to the TRE (Fig. S7C-D), ARF6 inactivation is unlikely to lie downstream of PIKfyve mislocalization by FTY720 or 893. Together, these data support the model that PP2A activation leads to ARF6 inactivation and a block in endocytic recycling.

If PP2A activation is upstream of ARF6 inactivation, then inhibition of PP2A should maintain ARF6-GTP levels in sphingolipid-treated cells. Unexpectedly, the PP2A inhibitor calyculin A that blocked transporter internalization and restored endocytic recycling (Fig. 2E-G) inactivated ARF6 even in the absence of exogenous sphingolipids (Fig. 5H). This result may reflect the fact that PP2A is a heterotrimeric enzyme that can take over 50 different forms with distinct subunit composition and

substrate preferences (Sangodkar et al., 2016). Sphingolipids may activate only a subset of PP2A isoforms, but calyculin A inhibits all PP2A heterotrimers, including sphingolipid-insensitive PP2A heterotrimers that might promote ARF6 activation. Off-target effects on proteins other than PP2A may also contribute to the inactivation of ARF6 by calyculin A. Our efforts to measure ARF6-GTP levels in cells where PP2A was genetically inhibited were unsuccessful. Loss of PP2A catalytic activity is cell lethal, and sufficient quantities of viable cells with PP2A-A or PP2A-C subunit knockdown could not be generated for use in effector pulldown assays. Knocking down individual PP2A-B subunits was a less-toxic approach, but failed to protect cells from transporter loss (data not shown). While SV40 small t antigen blocked sphingolipid-induced nutrient transporter loss in transient transfection assays (Kim et al., 2016), expression levels achieved in stable populations or cell clones were not sufficient to protect against transporter loss; similar results were obtained in cells stably overexpressing the PP2A inhibitor I$_2$PP2A/SET (data not shown). Given these technical difficulties, a definitive test of whether ARF6 inactivation lies downstream of sphingolipid-induced PP2A activation will require additional mechanistic insight. Nonetheless, the correlation between the ability of sphingolipids to trigger nutrient transporter loss, starve cells, reduce ARF6-GTP levels and activate PP2A suggests that PP2A activation is likely to be upstream of ARF6 inactivation.

ARF6 inactivation is necessary and sufficient to account for reduced nutrient transporter recycling in sphingolipid-treated cells

Dominant-negative and constitutively active mutants are routinely used to study GTPase function. Constitutively active mutants exist preferentially in the GTP-bound state due to mutations that prevent GTP hydrolysis, whereas dominant-negative mutants are
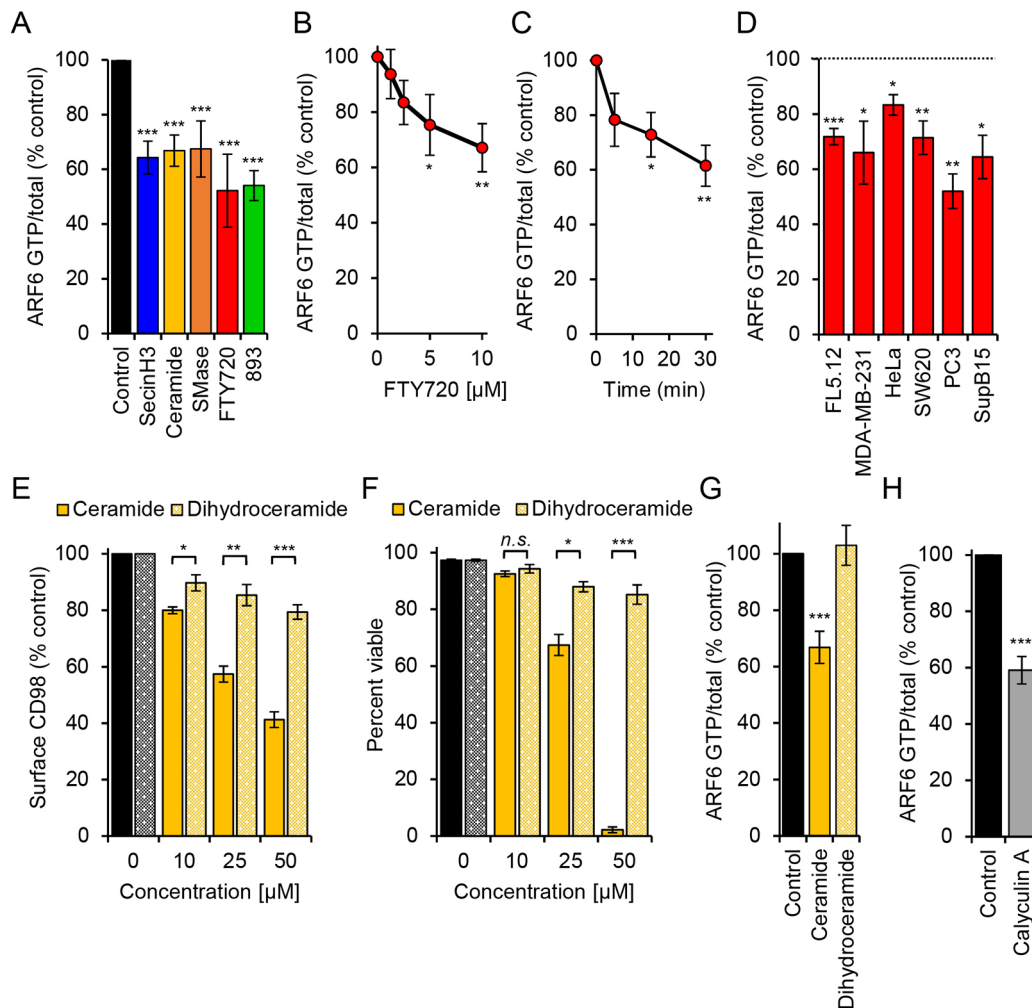
Fig. 5. Endogenous and synthetic sphingolipids that downregulate nutrient transporters also inactivate the ARF6 GTPase. (A) ARF6-GTP levels normalized to total ARF6 in FL5.12 cells treated with the cytohesin inhibitor SecinH3 (30 µM), C_2-ceramide (50 µM), bacterial sphingomyelinase (bSMase; 100 mU/ml), FTY720 (5 µM) or 893 (5 µM) for 3 h. (B,C) ARF6-GTP levels in FL5.12 cells treated with FTY720 (0, 1.25, 2.5, 5 or 10 µM) for 30 min (B) or with 10 µM FTY720 for 5, 15 or 30 min (C). (D) ARF6-GTP levels in FL5.12, MDA-MB-231, HeLa, SW620, PC3 or SupB15 treated for 3 h with FTY720 (10 µM). (E) Steady state surface CD98 levels in FL5.12 cells treated with C_2-ceramide or C_2-dihydroceramide at the indicated concentrations for 3 h. (F) Viability of C_2-ceramide- or C_2-dihydroceramide-treated FL5.12 cells at 48 h. (G) ARF6-GTP levels in FL5.12 cells treated with C_2-ceramide (50 µM) or C_2-dihydroceramide (50 µM). (H) ARF6-GTP levels in FL5.12 cells treated with CalyculinA (10 nM) for 1 h. Means±s.e.m. shown of $n \geq 3$ in all panels. Using two-tailed t-test (D-F,H) or ordinary one-way ANOVA (A-C,G): n.s., not significant; $*P \leq 0.05$; $**P \leq 0.01$; $***P \leq 0.001$. Dunnett's test was used to correct for multiple comparisons (A-C,G). See also Fig. S5.

preferentially in the GDP-bound state and compete with the endogenous GTPase for GEFs. While these mutants can provide key insights, GTPase cycling between the GDP- and GTP-bound forms is required for normal GTPase function. Indeed, the constitutively active ARF6 mutant ARF6-Q67L causes nutrient transporter proteins to accumulate intracellularly in large, perinuclear vesicles and, not surprisingly, failed to restore nutrient transporters to the surface in sphingolipid-treated cells (Eyster et al., 2009 and not shown). However, consistent with our finding that sphingolipids inactivate ARF6, the dominant-negative mutant ARF6-T27N drove CD98 into tubular endosomes and cytoplasmic puncta similar to the phenotype in sphingolipid-treated cells (Fig. 3A, Fig. 4B and Fig. 6A,B). ARF6-T27N also mislocalized the recycling cargo TGN46 to peripheral vesicular structures, suggesting that ARF6 inactivation was sufficient to explain the recycling defects observed with sphingolipids (Fig. S7E). Both the cytohesin inhibitor SecinH3 and the allosteric ARF6 inhibitor NAV2729 also disrupted the localization pattern of

CD98 (Fig. 6C,D) and TGN46 (Fig. S7F) and phenocopied the effects of sphingolipids on MICAL-L1, eliminating tubular MICAL-L1 localization (Fig. 6F) and blocking ARF6 and RAB35 recruitment to the TRE in a similar manner to 893 and ceramide (Fig. S6A-C). If ARF6 activity is necessary for nutrient transporter recycling from the TRE, then reducing ARF6-GTP with SecinH3 should recapitulate the recycling block induced by sphingolipids. To measure recycling, HeLa cells were treated with ceramide or 893 to induce CD98 and GLUT1 internalization and cytoplasmic levels of transporters were compared with levels in untreated control cells (Fig. 6G). Washing out sphingolipids after 1 h reduced the amount of intracellular transporter analogous to results obtained in SupB15 leukemia cells (Fig. 2C and Fig. 6G). Inclusion of SecinH3 in the medium after 893 or ceramide washout was sufficient to retain both CD98 and GLUT1 in swollen endosomal structures (Fig. 6G). Taken together, genetic and small-molecule inhibitor studies indicate that reducing ARF6-GTP levels is sufficient to account for the sphingolipid-induced defect in nutrient transporter recycling.
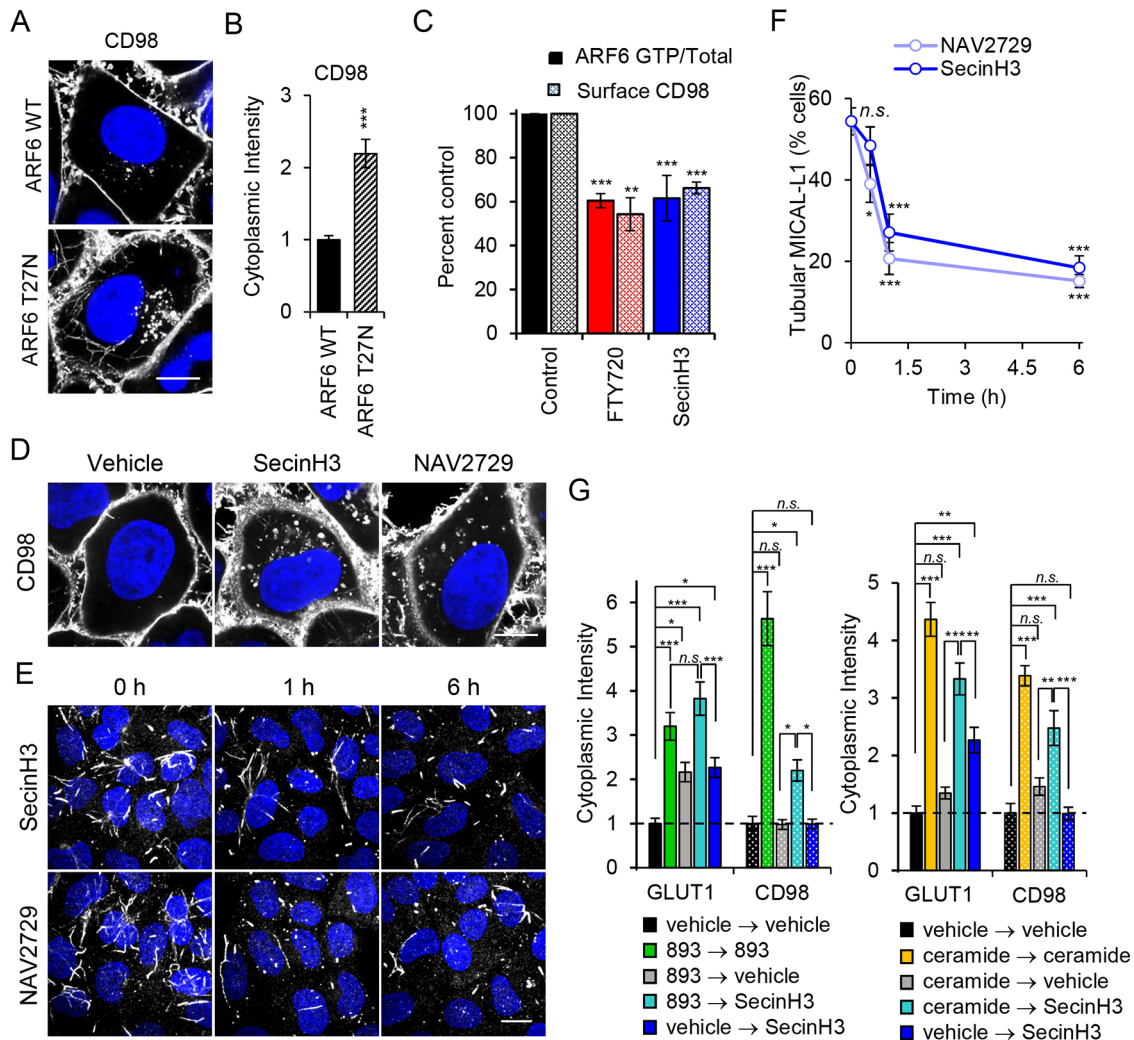
Fig. 6. ARF6 inactivation is sufficient to inhibit nutrient transporter recycling. (A) HeLa cells expressing HA-ARF6 or HA-ARF6-T27N stained for CD98. (B) Quantification of intracellular CD98 intensity in A. (C) Surface CD98 quantification and ARF6-GTP levels in FL5.12 cells treated with FTY720 (5 µM) or SecinH3 (30 µM) for 3 h. (D) HeLa cells treated with SecinH3 (30 µM) or NAV2729 (12.5 µM) for 16 h and stained for CD98. (E) HeLa cells treated with SecinH3 (30 µM) or NAV2729 (12.5 µM) for 1 or 6 h and stained for MICAL-L1. (F) Quantification of E. (G) Cytoplasmic intensity quantification of CD98 and GLUT1 in HeLa cells treated with vehicle, 893 (10 µM), or C_2-ceramide (50 µM) for 1 h, washed with PBS, then returned to 893 (10 µM) or placed in vehicle or SecinH3 (30 µM) for 2 h. Means±s.e.m. shown for $n{\geq}3$ in all panels. Using a two-tailed t-test (B) or an ordinary one-way ANOVA (C,F,G) to compare treated samples with controls: n.s., not significant; $*P{\leq}0.05$; $**P{\leq}0.01$; $***P{\leq}0.001$. Dunnett's test was used in C,F and Tukey's test was used in G to correct for multiple comparisons. Scale bars: 10 µm. See also Figs S6 and S7.

To determine whether ARF6 inactivation was necessary for sphingolipid-induced nutrient transporter loss, we attempted to maintain ARF6-GTP in sphingolipid-treated cells. As mentioned above, the ARF6 GTPase cycle is critical for its normal function and the constitutively active ARF6-Q67L mutant disrupts rather than facilitates ARF6-dependent recycling (Cohen et al., 2007; D'Souza-Schorey et al., 1998; Donaldson, 2003; Donaldson et al., 2009; Eyster et al., 2009; Maldonado-Báez et al., 2013; Santy, 2002). Overexpression of ARF6 GEFs is commonly employed as a more physiological means to activate ARF6 (Cohen and Donaldson, 2010; Kanamarlapudi, 2014; Santy and Casanova, 2001). However, GEF overexpression can also lead to ARF6 hyperactivation, inducing abnormal, non-physiological phenotypes similarly to the ARF6-Q67L mutant (Cohen et al., 2007; Li et al., 2012; Monier et al., 1998). The PH domain of SLM proteins bears significant homology to the PH domain of cytohesin family GEFs, the cytohesin inhibitor SecinH3 recapitulated many of the effects of

sphingolipids on endocytic trafficking (Fig. 6C-G),and cytohesin-3 (GRP1) promotes GLUT4 recycling in response to insulin (Li et al., 2012). Thus, we attempted to maintain ARF6-GTP levels in sphingolipid-treated cells by overexpressing GRP1. GRP1 is activated by insulin-dependent AKT-mediated phosphorylation of Ser155 and Thr280 (Li et al., 2012). Because we suspected that PP2A activation was upstream of ARF6 inactivation, a constitutively active, phosphomimetic mutant where these serine and threonine residues were converted to aspartic acid (GRP1-DD) was also evaluated. HeLa cells were transfected with GFP (negative control), wild-type GRP1, or GRP1-DD and CD98 localization with or without 893 was monitored by immunofluorescence microscopy. As expected, 893 downregulated CD98 in GFP-expressing cells leading to its accumulation in swollen endocytic structures (Fig. 7A). Overexpression of wild-type GRP1 led to an unexpected phenotype: CD98 was no longer evenly distributed along the plasma membrane but rather collected in membrane
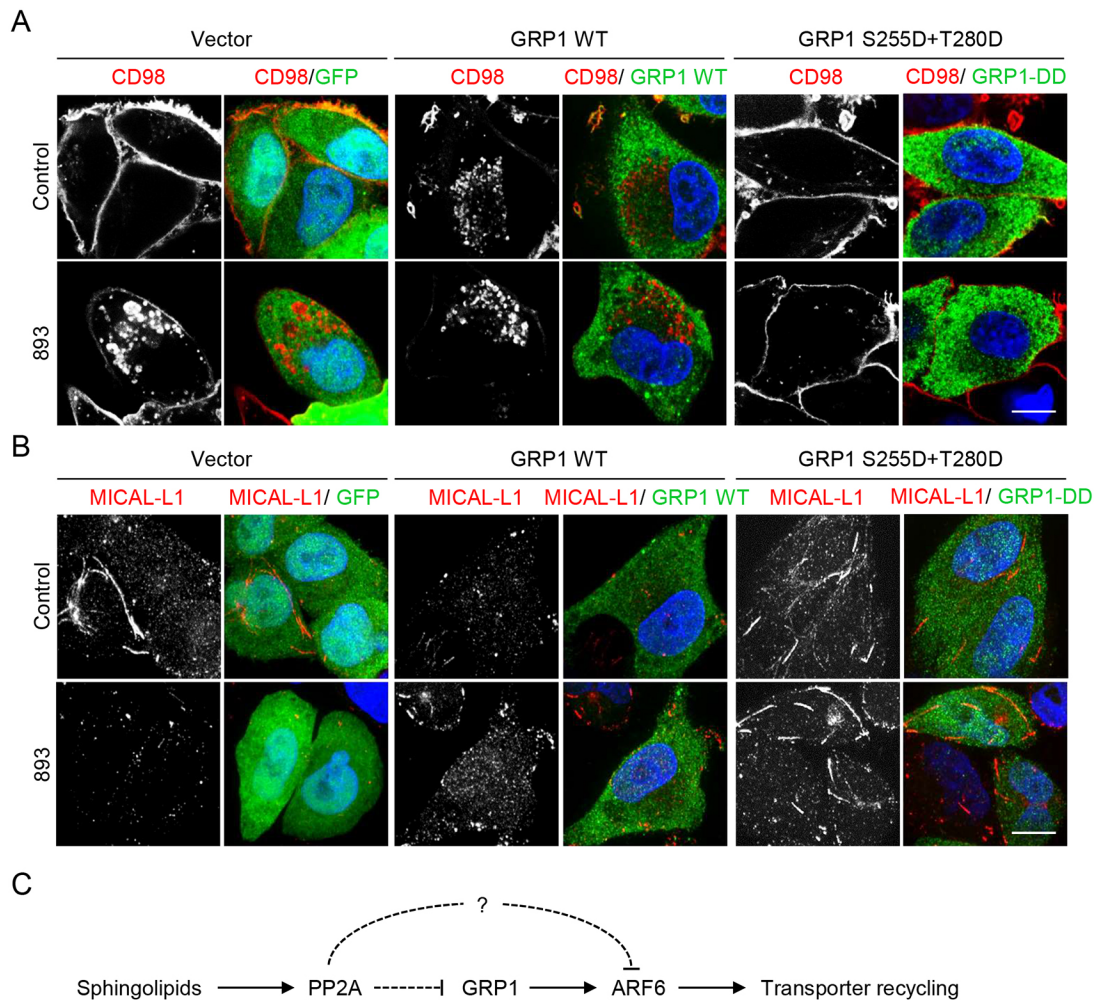
Fig. 7. A phosphomimetic mutant of GRP1 protects nutrient transporter recycling from inhibition by 893. (A) HeLa cells expressing GFP alone, myc-tagged wild-type GRP1, or myc-tagged GRP1 S155D+T280D (GRP1-DD) were treated with 893 (5 µM) for 6 h and stained for GFP or myc tag and CD98. (B) As in A, except cells were stained for MICAL-L1 and myc tag or GFP. Scale bars: 10 µm. (C) Model for regulation of endocytic recycling by sphingolipids.

ruffles and in small endosomes that accumulated in the perinuclear region. While CD98 localization to plasma membrane ruffles was not observed in cells expressing the activated mutant ARF6-Q67L, accumulation of CD98 in perinuclear vesicles is consistent with ARF6 hyperactivation (data not shown and Eyster et al., 2009). Given its basal effects on CD98 localization, it was not surprising that overexpression of wild-type GRP1 failed to protect from sphingolipid-induced nutrient transporter loss (Fig. 7A). Intriguingly, CD98 localization was not basally altered in GRP1-DD-expressing cells despite the reported constitutive activity of this mutant (Fig. 7A and Li et al., 2012); sequencing of the plasmids used in this experiment confirmed the identity of the wild-type and mutant constructs. The increased localization of GRP1-DD to endosomes might contribute to its differential activity (Li et al., 2012). Importantly, GRP1-DD eliminated the endosomal CD98 signal in 893-treated cells (Fig. 7A), suggesting that GRP1-DD might maintain recycling in sphingolipid-treated cells. Given that ARF6 inhibition destabilizes the TRE and GRP1-DD restores recycling, this mutant might also stabilize the TRE in 893-treated cells. Indeed, while MICAL-L1-positive tubules were absent in GFP- and GRP1-expressing cells exposed to 893, MICAL-L1 tubules were readily detectable in GRP1-DD-expressing cells exposed to 893 (Fig. 7B). Disappointingly, populations or clones

stably expressing GRP1-DD had markedly lower expression levels of exogenous GRP1 compared with the transient overexpressing cells and were not protected from CD98 loss (data not shown). As a result, the ability of GRP1-DD to rescue cells from 893-induced ARF6 inactivation and cell death could not be evaluated. Moreover, changes in GRP1 phosphorylation in response to sphingolipids could not be detected using an antibody that recognizes phosphorylated AKT substrates (Li et al., 2012) (data not shown). In summary, these studies suggest that sphingolipids disrupt endocytic recycling by activating PP2A and inactivating ARF6 (Fig. 7C).

ARF6 inhibition contributes to the anti-neoplastic effects of synthetic sphingolipids

Sphingolipids selectively kill cancer cells, in part, by starving them secondary to nutrient transporter downregulation (Guenther et al., 2008; Kim et al., 2016; Romero Rosales et al., 2011). If ARF6 inactivation blocks access to nutrients by limiting nutrient transporter recycling, then small molecules that inactivate ARF6 may sensitize cancer cells to suboptimal non-cytotoxic concentrations of anti-neoplastic sphingolipids. In SupB15 leukemia cells, SecinH3 was not cytotoxic or even cytostatic as a single agent (Fig. 8A and not shown). At 5 µM, FTY720 blocked
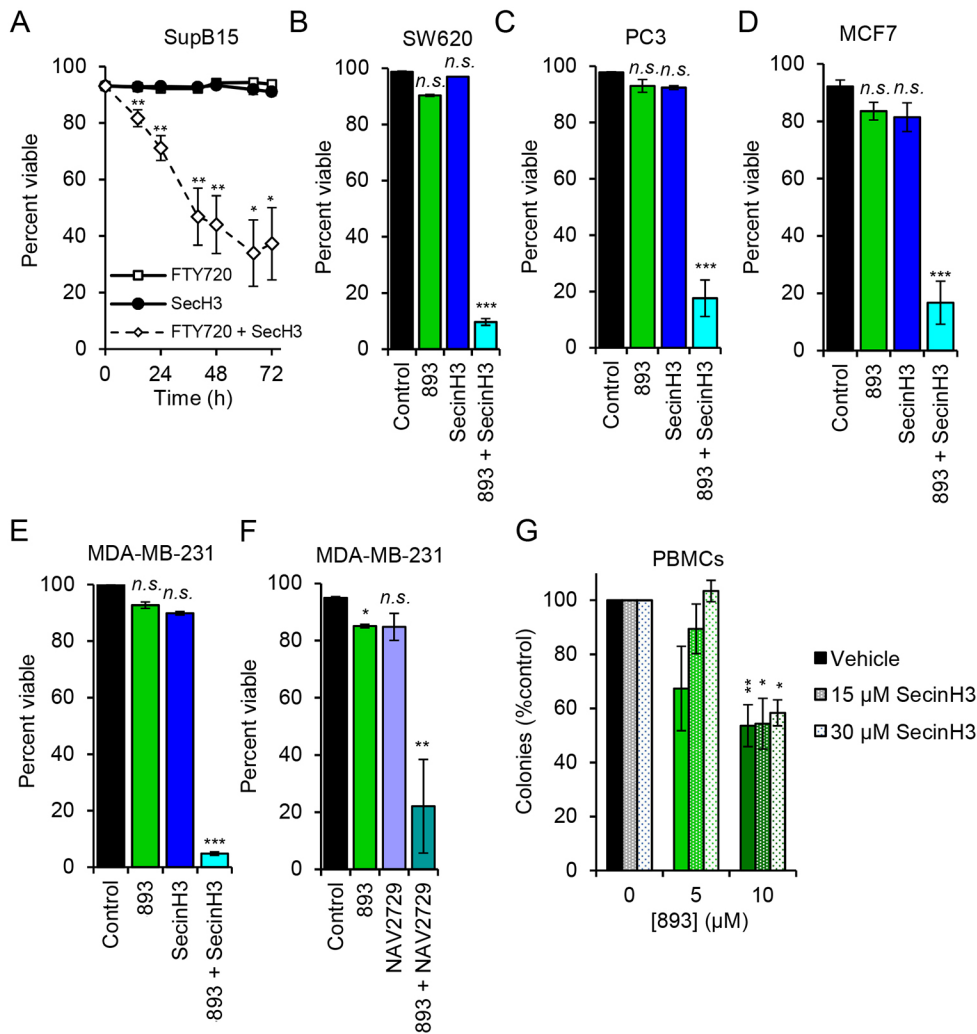
Fig. 8. ARF6 inhibition enhances the anti-neoplastic effects of synthetic sphingolipids. (A) Viability of SupB15 cells treated with FTY720 (5 µM), SecinH3 (30 µM) or both. (B-E) Viability of different cell lines treated with 893 (4 µM), SecinH3 (30 µM) or a combination. (B) SW620 cells at 120 h. (C) PC3 cells at 144 h. (D) MCF7 cells at 120 h. (E) MDA-MB-231 cells at 96 h. (F) MDA-MB-231 cells at 96 h treated with 893 (4 µM) and NAV2729 (6.25 µM). (G) Peripheral blood mononuclear cell (PBMC) colony formation assay at the indicated doses of 893 and SecinH3. Means±s.e.m. shown for $n{\geq}3$ in all panels. Using two-tailed t-test (A) or ordinary one-way ANOVA (B-G) to compare with controls: n.s., not significant; *$P{\leq}0.05$; **$P{\leq}0.01$; ***$P{\leq}0.001$. Tukey's test was used to correct for multiple comparisons in B-G; statistics are relative to the respective control.

SupB15 cell proliferation but did not induce cell death. However, the combination of 5 µM FTY720 with a dose of SecinH3 that inactivates ARF6 (Fig. 5A) killed >60% of the leukemia cells in 72 h (Fig. 8A). As a single agent, SecinH3 did not affect the proliferation or viability of SW620 colorectal cancer cells, PC3 prostate cancer cells, MDA-MB-231 breast cancer cells or MCF7 breast cancer cells (Fig. 8B-E and data not shown). However, in each of these cell lines, SecinH3 dramatically potentiated the effect of a suboptimal concentration of 893 suggesting that ARF6 inactivation contributes to sphingolipid-induced cell death. Similar results were obtained with the allosteric ARF6 inhibitor NAV2729 in MDA-MB-231 cells (Fig. 8F). *In vitro*, cancer cells are at least 10-fold more sensitive than non-transformed cells to the cytotoxic effects of 893, most likely because their oncogenic mutations drive anabolism and limit their ability to make adaptive metabolic changes that would compensate for reduced nutrient access (Kim et al., 2016). To test whether combining SecinH3 with 893 would reduce or expand this therapeutic index, colony formation by peripheral blood mononuclear cells was measured in the presence or absence of SecinH3 and 893. In contrast to our results in five different human cancer cell lines (Fig. 8A-E), SecinH3 did not sensitize PBMCs to 893 (Fig. 8G). In fact, SecinH3 may have partially protected normal cells from 893 although this effect was not statistically significant. These studies suggest that ARF6 inactivation contributes to the anti-neoplastic activity of

sphingolipids and that combining ARF6 inhibitors with 893 could extend the dose range over which 893 is effective without increasing toxicity to normal proliferating cells.

DISCUSSION

While we and others have previously shown that a subset of sphingolipids downregulate glucose and amino acid transporters (Barthelemy et al., 2017; Bultynck et al., 2006; Chung et al., 2001; Guenther et al., 2008; Kim et al., 2016; Romero Rosales et al., 2011; Skrzypek et al., 1998; Summers et al., 1998), the molecular mechanism is incompletely defined. As restricting nutrient access is a key mode of action for both endogenous and synthetic anti-neoplastic sphingolipids, understanding the molecular mechanism underlying this phenotype will provide insight into normal cell biology and clarify which tumor cells will be sensitive and resistant to therapeutic approaches that involve sphingolipid delivery or generation. Studies in yeast suggest that both internalization and recycling of nutrient transporter proteins are affected by sphingolipids (Barthelemy et al., 2017; Bultynck et al., 2006; Chung et al., 2001; Kamble et al., 2011; Welsch et al., 2004). The work presented here demonstrates that sphingolipids block transporter recycling in mammalian cells. While the molecular details of sphingolipid-induced nutrient transporter loss differ between yeast and mammalian cells, there are several interesting parallels. SLM1/2 are localized to both the plasma membrane and eisosomes, structures composed of

multiple BAR domain proteins that promote membrane tubulation and endocytosis (Olivera-Couto et al., 2011). Intriguingly, expression of yeast eisosome proteins in COS-7 cells resulted in a tubular staining pattern highly reminiscent of the MICAL-L1-positive TRE (Olivera-Couto et al., 2011). While the precise molecular relationships between the yeast and mammalian sphingolipid-responsive pathways are not yet clear, it is interesting to speculate that the eisosome endocytic recycling pathway is paralleled in mammalian cells by the ARF6-dependent TRE.

Although overexpression of a phosphomimetic mutant of GRP1 (GRP1-DD) rescued from both sphingolipid-induced nutrient transporter downregulation and loss of the MICAL-L1-positive TRE (Fig. 7A,B), other ARF6 regulatory proteins may be affected by sphingolipids (Fig. 7C). For example, RAB35-GTP negatively regulates ARF6 activity by recruiting the ARF6 GAP ACAP2 to the recycling endosome (Chesneau et al., 2012; Kobayashi and Fukuda, 2012; Rahajeng et al., 2012). RAB35 activation also leads to the loss of MICAL-L1-positive tubular endosomes similar to what was observed in sphingolipid-treated cells (Fig. 3C-F and Fig. 4A) (Rahajeng et al., 2012). However, using a published RAB35 effector pull-down assay (Chesneau et al., 2012), we were unable to detect reproducible changes in RAB35-GTP levels following sphingolipid treatment (not shown). This negative result is consistent with our finding that ACAP2 siRNA did not restore ARF6-GTP levels or CD98 trafficking in sphingolipid-treated cells (not shown). We were unable to demonstrate that PP2A activation is necessary for sphingolipid-induced ARF6 inactivation. However, the inability of C_2-dihydroceramide to activate PP2A (Chalfant et al., 2004; Kim et al., 2016) or trigger trafficking disruptions associated with ARF6 inactivation, our finding that the non-sphingolipid small molecule PP2A activator perphenazine (PPZ) recapitulates phenotypes associated with ARF6 inactivation and the selective protection from sphingolipid-induced phenotypes by a phosphomimetic GRP1 mutant all provide support for the model shown in Fig. 7C.

ARF6 has multiple pro-oncogenic roles, and establishing a connection between tumor suppressive sphingolipids and this GTPase has implications beyond the effects on nutrient transporter trafficking. ARF6 activity is important for primary tumor growth in some models, although the mechanism is incompletely defined and may vary with tumor type. ARF6 is activated downstream of a variety of receptor tyrosine kinases that drive tumor growth (Hongu et al., 2015; Hu et al., 2013; Li et al., 2017; Morishige et al., 2008). ARF6 promotes recycling of the MET receptor tyrosine kinase (Parachoniak et al., 2011), and thus decreasing ARF6-GTP may reduce MET surface levels with important consequences for the highly invasive MET-driven cancers like hereditary kidney cancers, sporadic papillary renal cancer, hepatocellular carcinoma, and gastric cancer (Boccaccio and Comoglio, 2006; Danilkovitch-Miagkova and Zbar, 2002). MET and ARF6 promote tumor angiogenesis by stimulating β1-integrin recycling in a GRP1-dependent manner (Hongu et al., 2015). Melanoma and lung tumor isograft growth is compromised in mice lacking ARF6 selectively in endothelial cells, and treatment with the cytohesin inhibitor SecinH3 limited tumor growth and blocked angiogenesis in vivo (Bill et al., 2012; Hongu et al., 2015). SecinH3 has also been shown to limit primary tumor growth in other situations, including breast cancer and colorectal cancer models (Pan et al., 2014; Zhao et al., 2016). The structurally unrelated allosteric ARF6 inhibitor NAV-2729 was recently shown to inhibit tumor growth in a uveal melanoma model (Yoo et al., 2016). These studies with small-molecule ARF6 inhibitors indicate that ARF6 is an actionable target in cancer. The results presented here suggest

that endogenous sphingolipids and sphingolipid-like small molecules such as 893 may selectively kill cancer cells in part through ARF6 inactivation (Fig. 8; Kim et al., 2016). Moreover, sphingolipid-like agents or chemotherapies that increase ceramide generation (Dimanche-Boitrel et al., 2011; Morad and Cabot, 2013; Ogretmen and Hannun, 2001, 2004) may be even more effective when used in combination with SecinH3 or NAV-2729.

ARF6 also has a well-documented role in metastasis in breast cancer, melanoma and clear-cell renal carcinoma (Grossmann et al., 2013; Hashimoto et al., 2004, 2016; Hu et al., 2013; Loskutov et al., 2015; Morishige et al., 2008; Muralidharan-Chari et al., 2009a,b; Tague et al., 2004; Yoo et al., 2016). Invadopodia are actin-rich cellular protrusions enriched with various matrix proteases that form cell-ECM contacts for matrix degradation and subsequent tumor cell intravasation into the vasculature (Paz et al., 2014). ARF6 activity is required for invadopodia formation and subsequent localized matrix degradation (Hashimoto et al., 2004). Membrane-tethered membrane type 1-matrix metalloproteinase (MT1-MMP) is secreted from cancer cells and promotes metastasis secondary to collagen breakdown (Marchesin et al., 2015; Paz et al., 2014; Sodek et al., 2007). ARF6 activity promotes recycling of MT1-MMP to the plasma membrane for release to the extracellular matrix (Loskutov et al., 2015; Marchesin et al., 2015). Lastly, tumor-derived microvesicles can promote angiogenesis, immune suppression, tumor invasion and metastasis (D'Souza-Schorey and Clancy, 2012). ARF6 activation also promotes the release of microvesicles containing matrix proteases such as MT1-MMP (Muralidharan-Chari et al., 2009b). Given the multifaceted roles of ARF6 in tumor cell invasion and metastasis, whether ceramide and synthetic sphingolipids such as 893 limit metastasis as a consequence of ARF6 inactivation merits further evaluation.

MATERIALS AND METHODS
Cell culture
SupB15, MDA-MB-231, SW620 and PC3 cells were obtained from the ATCC. Normal, non-transformed hematopoietic FL5.12 cells were obtained from Craig B. Thompson (Memorial Sloan Kettering Cancer Center, New York, NY, USA), HeLa cells from Steve Caplan (University of Nebraska Medical Center, Omaha, NE, USA) and MCF7 cells from the Translational Oncology Research Laboratory at UCLA (University of California Los Angeles, Los Angeles, CA, USA). PBMCs were obtained through the CTSA-supported Institute for Clinical and Translational Science at UCI under IRB protocols 2015-1883 (Edinger) and 2001-2058 (ICTS). FL5.12 and SupB15 cells were maintained in RPMI 1640 supplemented with 10% fetal bovine serum (FBS), 10 mM HEPES, 55 μM β-mercaptoethanol, 2 mM L-glutamine and 1% antibiotics. FL5.12 medium was additionally supplemented with 500 pg/ml recombinant murine IL-3. HeLa cells were maintained in DMEM with 4.5 g/l glucose and L-glutamine supplemented with 10% FBS and antibiotics. MDA-MB-231 and SW620 cells were cultured in DMEM containing 4.5 g/l glucose and L-glutamine supplemented with 10% FBS, 1 mM sodium pyruvate and antibiotics. PC3 cells were cultured in F12-K medium supplemented with 10% FBS and antibiotics. MCF7 cells were cultured in RPMI 1640 supplemented with 10% FBS and 1% antibiotics. Cells were screened for Mycoplasma contamination at least every 6 months using the LookOut Mycoplasma PCR Detection Kit (Sigma, Cat# MP0035-1KT); the cell lines utilized in this study tested negative in all screens.

Antibodies
Antibodies were purchased from BD Biosciences (PE Rat IgG1 κ isotype Cat #551979, flow cytometry 1:400 dilution; unconjugated anti-mouse CD98 Cat #557479, flow cytometry 1:400 dilution; unconjugated anti-human CD98 Cat #556074, flow cytometry and IF 1:100 dilution; unconjugated Mu IgG1 κ isotype Cat #554121, flow cytometry 1:100

dilution; PE anti-human CD98 Cat #556077, flow cytometry 1:100 dilution; PE Mu IgG1 κ isotype Cat #555749, flow cytometry 1:100 dilution; transferrin Receptor/CD71 Cat# 555534, IF 1:100 dilution); Biolegend (PE anti-mouse CD98, Cat #128208, flow cytometry 1:400 dilution; unconjugated anti-mouse CD98, Cat #128202, flow cytometry 1:400 dilution); Cell Signaling Technology (ARF6 Cat #5740, WB 1:1000 dilution; HA-tag Cat #2367, WB 1:1000, IF 1:100 dilution; EEA1 Cat# 3288, IF 1:100 dilution; Lamp1 Cat# 9091, IF 1:200 dilution; GM130 Cat#12480, IF 1:100 dilution); Novus Biologicals (MICAL-L1 Cat# H00085377-B01P, IF 1:100 dilution, WB 1:1000 dilution; GLUT1 Cat# NB300-666, IF 1:100 dilution); LI-COR (IRDye 800CW Gt-α-Rb Cat #92632211, WB 1:10,000 dilution; IRDye 680LT Gt-α-Mu Cat #926-68020, WB 1:10,000 dilution; IRDye 800CW Dk-α-Gt Cat #926-32214, WB 1:10,000 dilution; IRDye 800CW Gt-α-Mu Cat #926-32210, WB 1:10,000 dilution; IRDye 800CW Gt-α-Rt Cat #926-32219, WB 1:10,000 dilution; IRDye 680LT Dk-α-Rb Cat #926-68023, WB 1:10,000 dilution); BIO-RAD (TGN46 Cat #AHP500G, IF 1:100 dilution); Invitrogen (Alexa Fluor 488 goat anti-mouse IgG Cat #A-11029, IF 1:200 dilution; Alexa Fluor 488 goat anti-rabbit IgG Cat #A-11008, IF 1:200 dilution; Alexa Fluor 488 donkey anti-sheep IgG Cat #A-11015, IF 1:200 dilution; Alexa Fluor 594 goat anti-mouse IgG Cat #A-11032, IF 1:200 dilution; Alexa Fluor 594 donkey anti-mouse Cat #A-21203, IF 1:200 dilution; Alexa Fluor 594 goat anti-rabbit Cat #R37117, IF 1:200 dilution).

Chemicals
C2-ceramide (VWR Cat #89164-564); dihydro-C2-ceramide (VWR Cat #89164-568); FTY720 (Fisher Cat #50148635); cantharidin (VWR Cat #89147-162); calyculinA (VWR Cat #89157-750); tautomycin (VWR Cat #89149-880); YM201636 (Cayman Chemical Cat #13576); SecinH3 (Cayman Chemical Cat #10009570); NAV2729 (Tocris Cat #5986). The enzyme bacterial sphingomyelinase (bSMase) was derived from S. aureus (Sigma Cat #S8633). SH-BC-893 (893) and the lactam version (893-lactam) were synthesized in Dr. Stephen Hanessian's lab at University of Montreal or by IntelliSyn RD, Montreal, Quebec, Canada.

Plasmids and transfection
GFP-tagged MICAL-L1 was a gift from Dr Steve Caplan (University of Nebraska Medical Center, Omaha, NE, USA); pCDNA3-HA-ARF6-WT, -ARF6-Q67L and -ARF6-T27N were generously provided by Julie Donaldson (NIH, Bethesda, USA). pEF6-Myc-GRP1-WT and -GRP1-S155D/T240D were gifts from Dr Victor W. Hsu (Harvard Medical School, Boston, MA, USA). Transient transfections were performed using a calcium phosphate transfection protocol as lipid transfection reagents interfere with the cellular response to sphingolipids (not shown).

Confocal microscopy
Microscopy samples were prepared by plating cells on glass coverslips, upon which cells were treated, fixed with 4% paraformaldehyde [10 min, room temperature (RT)], then permeabilized and blocked with block solution (10% FCS, 0.3% saponin, azide in PBS) (30 min, 37°C). Coverslips were incubated in block solution with primary antibody overnight, rocking, at 4°C, then washed once with wash solution (0.03% saponin and azide in PBS), twice with PBS, and incubated in secondary antibody at RT for 1 h while rocking. Cells were again washed, incubated in 1 mg/ml DAPI in wash solution, washed and mounted on slides using Vectashield Mounting Medium (Vector Laboratories, Cat #H-1000). Confocal microscopy images were collected with Zeiss LSM780 confocal microscope with Plan-Apochromat 63×/1.40 Oil DIC or Plan-Apochromat 100×/1.40 Oil DIC objectives and using Zeiss ZEN digital imaging software. ImageJ software was used for image processing. All images were collected with the same microscope and image processing settings. Cytoplasmic intensity in Fig. 6B and G was measured using ImageJ. A region of interest (ROI) beneath the plasma membrane and excluding the nucleus was selected and the mean gray value (MGV) measured. Fluorescence intensity is expressed as the MGV within the ROI after subtracting the background MGV. To measure the percentage of cells containing tubular MICAL-L1 staining (Fig. 3D, Fig. 6F, Fig. S7B),

at least 20 different fields of view containing between 5 and 10 cells each were measured.

Flow cytometry
Viability was measured by vital dye exclusion using 1 mg/ml DAPI. For CD98 surface staining, 50,000-200,000 cells were incubated for 30 min on ice with primary antibody diluted in FACS block (10% FBS and 0.05% NaN_3 in PBS). Cells were washed twice with FACS wash (2% FBS and 0.05% NaN_3 in PBS) and suspended in FACS wash containing 1 mg/ml DAPI. Analysis was restricted to live cells. For the transferrin internalization assay, 100,000 cells were incubated on ice for 1 h with biotinylated transferrin (100 µg/ml, Thermo Fisher Cat #T23363) in blocking buffer (1% BSA in PBS). Cells were washed twice with blocking buffer, resuspended in complete growth medium on ice, and warmed to 37°C for the indicated intervals. Following internalization, cells were fixed with 1% paraformaldehyde and stained with APC-tagged streptavidin (Thermo Fischer, Cat #SA1005). For the transferrin recycling assay, cells were incubated with vehicle or FTY720 (5 µM) and Alexa Fluor 488-transferrin (1 µg/ml; Life Technologies, Cat #T13342). Following internalization, cells were resuspended in vehicle or FTY720 without transferrin for the indicated intervals. Surface transferrin was stripped with pH 5.0 buffer. Samples were evaluated on a Becton Dickinson LSRII flow cytometer.

Measurement of ARF6-GTP levels
ARF6-GTP was quantified as previously described (Cohen and Donaldson, 2010). Briefly, pGEX plasmid expressing GST (control) or GST-VHS-GAT (effector pull-down construct) was transformed into BL21 cells. Protein expression was induced with IPTG (0.6 mM). Proteins were isolated using glutathione Sepharose 4B beads (Sigma-Aldrich, Cat #17-0756-01). Protein was quantified using a BCA assay (Thermo Scientific Cat #23223). Depending on ARF6 protein expression level, 50-200 µg cell lysate protein was combined with 40 µg of GST-bound or GST-GGA3-VHS-GAT-bound beads and rocked at 4°C for 1 h. Beads were washed three times with lysis buffer and protein eluted in 10 µl 2× NuPAGE loading buffer. Total ARF6 protein levels were evaluated using 10% of the pull-down lysate.

Western blotting
Cell lysates were prepared in Triton X-100 or RIPA lysis buffer containing 1× complete protease inhibitor (Roche, Cat #11697498001 or Pierce, Cat #88265). Protein concentration was quantified using Pierce BCA protein assay (Thermo Scientific, Cat #23223). Western blot samples were prepared in 1× NuPAGE sample buffer (Invitrogen, Cat #NP0007) supplemented with 1× protease inhibitor and 50 mM DTT. Samples were run on Invitrogen NuPAGE 4-12% Bis-Tris Gels (Cat #NP0336BOX) and transferred to BioTrace NT nitrocellulose membrane (Pall, Cat #66485). Nitrocellulose blots were incubated in blocking solution (5% bovine serum albumin, 0.05% NaN_3 in 1× TBST) for 1 h then incubated overnight at 4°C in blocking solution containing primary antibody at the recommended dilution. Blots were washed three times in 1× TBST (TBS with 0.1% Tween 20), incubated at RT for 1 h in blocking solution containing secondary antibody (1:10,000), then washed three times in TBST. Blots were imaged and quantified using a LI-COR Odyssey SA imaging system.

Author contributions
Conceptualization: B.T.F., M.U.R., E.M.S., A.L.E.; Methodology: B.T.F., M.U.R., E.M.S, A.N.M., A.L.E.; Validation: B.T.F., M.U.R.; Formal analysis: B.T.F., M.U.R., A.L.E.; Investigation: B.T.F., M.U.R., G.L., E.M.S., A.N.M., J.Y., Y.J., J.N., K.O., S.G.R., V.D.M., D.V.C.; Resources: A.L.E.; Data curation: B.T.F., M.U.R., A.L.E.; Writing - original draft: B.T.F., M.U.R., A.L.E.; Writing - review & editing: B.T.F.,

Supplementary information
Supplementary information available online at
http://jcs.biologists.org/lookup/doi/10.1242/jcs.213314.supplemental

References
Barthelemy, C., Barry, A. O., Twyffels, L. and André, B. (2017). FTY720-induced endocytosis of yeast and human amino acid transporters is preceded by reduction of their inherent activity and TORC1 inhibition. *Sci. Rep.* **7**, 13816.

Bill, A., Schmitz, A., König, K., Heukamp, L. C., Hannam, J. S. and Famulok, M. (2012). Anti-proliferative effect of cytohesin inhibition in gefitinib-resistant lung cancer cells. *PLoS ONE* **7**, e41179.

Boccaccio, C. and Comoglio, P. M. (2006). Invasive growth: a MET-driven genetic programme for cancer and stem cells. *Nat. Rev. Cancer* **6**, 637-645.

Brinkmann, V., Billich, A., Baumruker, T., Heining, P., Schmouder, R., Francis, G., Aradhye, S. and Burtin, P. (2010). Fingolimod (FTY720): discovery and development of an oral drug to treat multiple sclerosis. *Nat. Rev. Drug Discov.* **9**, 883-897.

Bultynck, G., Heath, V. L., Majeed, A. P., Galan, J.-M., Haguenauer-Tsapis, R. and Cyert, M. S. (2006). Slm1 and slm2 are novel substrates of the calcineurin phosphatase required for heat stress-induced endocytosis of the yeast uracil permease. *Mol. Cell. Biol.* **26**, 4729-4745.

Cai, B., Xie, S., Caplan, S. and Naslavsky, N. (2014). GRAF1 forms a complex with MICAL-L1 and EHD1 to cooperate in tubular recycling endosome vesiculation. *Front. Cell Dev. Biol.* **2**, 22.

Chalfant, C. E., Szulc, Z., Roddy, P., Bielawska, A. and Hannun, Y. A. (2004). The structural requirements for ceramide activation of serine-threonine protein phosphatases. *J. Lipid Res.* **45**, 496-506.

Chen, S., Li, L., Li, J., Liu, B., Zhu, X., Zheng, L., Zhang, R. and Xu, T. (2014). SEC-10 and RAB-10 coordinate basolateral recycling of clathrin-independent cargo through endosomal tubules in Caenorhabditis elegans. *Proc. Natl. Acad. Sci. USA* **111**, 15432-15437.

Chen, B., Roy, S. G., McMonigle, R. J., Keebaugh, A., McCracken, A. N., Selwan, E., Fransson, R., Fallegger, D., Huwiler, A., Kleinman, M. T. et al. (2016). Azacyclic FTY720 analogues that limit nutrient transporter expression but lack S1P receptor activity and negative chronotropic effects offer a novel and effective strategy to kill cancer cells in vivo. *ACS Chem. Biol.* **11**, 409-414.

Chesneau, L., Dambournet, D., Machicoane, M., Kouranti, I., Fukuda, M., Goud, B. and Echard, A. (2012). An ARF6/Rab35 GTPase cascade for endocytic recycling and successful cytokinesis. *Curr. Biol.* **22**, 147-153.

Chung, N., Jenkins, G., Hannun, Y. A., Heitman, J. and Obeid, L. M. (2000). Sphingolipids signal heat stress-induced ubiquitin-dependent proteolysis. *J. Biol. Chem.* **275**, 17229-17232.

Chung, N., Mao, C., Heitman, J., Hannun, Y. A. and Obeid, L. M. (2001). Phytosphingosine as a specific inhibitor of growth and nutrient import in Saccharomyces cerevisiae. *J. Biol. Chem.* **276**, 35614-35621.

Cohen, L. A. and Donaldson, J. G. (2010). Analysis of Arf GTP-binding protein function in cells. *Curr. Protoc. Cell Biol.* **8**, 14.12.1–14.12.17.

Cohen, L. A., Honda, A., Varnai, P., Brown, F. D., Balla, T. and Donaldson, J. G. (2007). Active Arf6 recruits ARNO/cytohesin GEFs to the PM by binding their PH domains. *Mol. Biol. Cell* **18**, 2244-2253.

Danilkovitch-Miagkova, A. and Zbar, B. (2002). Dysregulation of Met receptor tyrosine kinase activity in invasive tumors. *J. Clin. Invest.* **109**, 863-867.

Daquinag, A., Fadri, M., Jung, S. Y., Qin, J. and Kunz, J. (2007). The yeast PH domain proteins Slm1 and Slm2 are targets of sphingolipid signaling during the response to heat stress. *Mol. Cell. Biol.* **27**, 633-650.

Dickson, R. C., Nagiec, E. E., Skrzypek, M., Tillman, P., Wells, G. B. and Lester, R. L. (1997). Sphingolipids are potential heat stress signals in Saccharomyces. *J. Biol. Chem.* **272**, 30196-30200.

Dimanche-Boitrel, M.-T., Rebillard, A. and Gulbins, E. (2011). Ceramide in chemotherapy of tumors. *Recent Pat. Anticancer Drug Discov.* **6**, 284-293.

Dobrowsky, R. T., Kamibayashi, C., Mumby, M. C. and Hannun, Y. A. (1993). Ceramide activates heterotrimeric protein phosphatase 2A. *J. Biol. Chem.* **268**, 15523-15530.

Donaldson, J. G. (2003). Multiple roles for Arf6: sorting, structuring, and signaling at the plasma membrane. *J. Biol. Chem.* **278**, 41573-41576.

Donaldson, J. G. and Jackson, C. L. (2011). ARF family G proteins and their regulators: roles in membrane transport, development and disease. *Nat. Rev. Mol. Cell Biol.* **12**, 362-375.

Donaldson, J. G., Porat-Shliom, N. and Cohen, L. A. (2009). Clathrin-independent endocytosis: a unique platform for cell signaling and PM remodeling. *Cell. Signal.* **21**, 1-6.

Douglas, L. M. and Konopka, J. B. (2014). Fungal membrane organization: the eisosome concept. *Annu. Rev. Microbiol.* **68**, 377-393.

D'Souza-Schorey, C. and Clancy, J. W. (2012). Tumor-derived microvesicles: shedding light on novel microenvironment modulators and prospective cancer biomarkers. *Genes Dev.* **26**, 1287-1299.

D'Souza-Schorey, C., van Donselaar, E., Hsu, V. W., Yang, C., Stahl, P. D. and Peters, P. J. (1998). ARF6 targets recycling vesicles to the plasma membrane: insights from an ultrastructural investigation. *J. Cell Biol.* **140**, 603-616.

Eyster, C. A., Higginson, J. D., Huebner, R., Porat-Shliom, N., Weigert, R., Wu, W. W., Shen, R.-F. and Donaldson, J. G. (2009). Discovery of new cargo proteins that enter cells through clathrin-independent endocytosis. *Traffic* **10**, 590-599.

Fadri, M., Daquinag, A., Wang, S., Xue, T. and Kunz, J. (2005). The pleckstrin homology domain proteins Slm1 and Slm2 are required for actin cytoskeleton organization in yeast and bind phosphatidylinositol-4,5-bisphosphate and TORC2. *Mol. Biol. Cell* **16**, 1883-1900.

Ghosh, R. N., Mallet, W. G., Soe, T. T., McGraw, T. E. and Maxfield, F. R. (1998). An endocytosed TGN38 chimeric protein is delivered to the TGN after trafficking through the endocytic recycling compartment in CHO cells. *J. Cell Biol.* **142**, 923-936.

Giridharan, S. S. P., Cai, B., Naslavsky, N. and Caplan, S. (2012). Trafficking cascades mediated by Rab35 and its membrane hub effector, MICAL-L1. *Commun. Integr. Biol.* **5**, 384-387.

Giridharan, S. S. P., Cai, B., Vitale, N., Naslavsky, N. and Caplan, S. (2013). Cooperation of MICAL-L1, syndapin2, and phosphatidic acid in tubular recycling endosome biogenesis. *Mol. Biol. Cell* **24**, 1776-1790, S1.

Grant, B. D. and Donaldson, J. G. (2009). Pathways and mechanisms of endocytic recycling. *Nat. Rev. Mol. Cell Biol.* **10**, 597-608.

Grossmann, A. H., Yoo, J. H., Clancy, J., Sorensen, L. K., Sedgwick, A., Tong, Z., Ostanin, K., Rogers, A., Grossmann, K. F., Tripp, S. R. et al. (2013). The small GTPase ARF6 stimulates β-catenin transcriptional activity during WNT5A-mediated melanoma invasion and metastasis. *Sci. Signal.* **6**, ra14.

Guenther, G. G., Peralta, E. R., Rosales, K. R., Wong, S. Y., Siskind, L. J. and Edinger, A. L. (2008). Ceramide starves cells to death by downregulating nutrient transporter proteins. *Proc. Natl. Acad. Sci. USA* **105**, 17402-17407.

Guenther, G. G., Liu, G., Ramirez, M. U., McMonigle, R. J., Kim, S. M., McCracken, A. N., Joo, Y., Ushach, I., Nguyen, N. L. and Edinger, A. L. (2014). Loss of TSC2 confers resistance to ceramide and nutrient deprivation. *Oncogene* **33**, 1776-1787.

Hannun, Y. A. and Obeid, L. M. (2008). Principles of bioactive lipid signalling: lessons from sphingolipids. *Nat. Rev. Mol. Cell Biol.* **9**, 139-150.

Hashimoto, S., Onodera, Y., Hashimoto, A., Tanaka, M., Hamaguchi, M., Yamada, A. and Sabe, H. (2004). Requirement for Arf6 in breast cancer invasive activities. *Proc. Natl. Acad. Sci. USA* **101**, 6647-6652.

Hashimoto, S., Mikami, S., Sugino, H., Yoshikawa, A., Hashimoto, A., Onodera, Y., Furukawa, S., Handa, H., Oikawa, T., Okada, Y. et al. (2016). Lysophosphatidic acid activates Arf6 to promote the mesenchymal malignancy of renal cancer. *Nat. Commun.* **7**, 10656.

Hongu, T., Funakoshi, Y., Fukuhara, S., Suzuki, T., Sakimoto, S., Takakura, N., Ema, M., Takahashi, S., Itoh, S., Kato, M. et al. (2015). Arf6 regulates tumour angiogenesis and growth through HGF-induced endothelial β1 integrin recycling. *Nat. Commun.* **6**, 7925.

Hu, Z., Xu, R., Liu, J., Zhang, Y., Du, J., Li, W., Zhang, W., Li, Y., Zhu, Y. and Gu, L. (2013). GEP100 regulates epidermal growth factor-induced MDA-MB-231 breast cancer cell invasion through the activation of Arf6/ERK/uPAR signaling pathway. *Exp. Cell Res.* **319**, 1932-1941.

Kamble, C., Jain, S., Murphy, E. and Kim, K. (2011). Requirements of Slm proteins for proper eisosome organization, endocytic trafficking and recycling in the yeast Saccharomyces cerevisiae. *J. Biosci.* **36**, 79-96.

Kanamarlapudi, V. (2014). Exchange factor EFA6R requires C-terminal targeting to the plasma membrane to promote cytoskeletal rearrangement through the activation of ADP-ribosylation factor 6 (ARF6). *J. Biol. Chem.* **289**, 33378-33390.

Kim, S. M., Roy, S. G., Chen, B., Nguyen, T. M., McMonigle, R. J., McCracken, A. N., Zhang, Y., Kofuji, S., Hou, J., Selwan, E. et al. (2016). Targeting cancer metabolism by simultaneously disrupting parallel nutrient access pathways. *J. Clin. Invest.* **126**, 4088-4102.

Kobayashi, H. and Fukuda, M. (2012). Rab35 regulates Arf6 activity through centaurin-β2 (ACAP2) during neurite outgrowth. *J. Cell Sci.* **125**, 2235-2243.

Kowluru, A. and Metz, S. A. (1997). Ceramide-activated protein phosphatase-2A activity in insulin-secreting cells. *FEBS Lett.* **418**, 179-182.

Li, J., Malaby, A. W., Famulok, M., Sabe, H., Lambright, D. G. and Hsu, V. W. (2012). Grp1 plays a key role in linking insulin signaling to glut4 recycling. *Dev. Cell* **22**, 1286-1298.

Li, R., Peng, C., Zhang, X., Wu, Y., Pan, S. and Xiao, Y. (2017). Roles of Arf6 in cancer cell invasion, metastasis and proliferation. *Life Sci.* **182**, 80-84.

Loskutov, Y. V., Kozyulina, P. Y., Kozyreva, V. K., Ice, R. J., Jones, B. C., Roston, T. J., Smolkin, M. B., Ivanov, A. V., Wysolmerski, R. B. and Pugacheva, E. N. (2015). NEDD9/Arf6-dependent endocytic trafficking of matrix metalloproteinase 14: a novel mechanism for blocking mesenchymal cell invasion and metastasis of breast cancer. *Oncogene* **34**, 3662-3675.

Maldonado-Báez, L., Williamson, C. and Donaldson, J. G. (2013). Clathrin-independent endocytosis: a cargo-centric view. *Exp. Cell Res.* **319**, 2759-2769.

Marchesin, V., Castro-Castro, A., Lodillinsky, C., Castagnino, A., Cyrta, J., Bonsang-Kitzis, H., Fuhrmann, L., Irondelle, M., Infante, E., Montagnac, G. et al. (2015). ARF6-JIP3/4 regulate endosomal tubules for MT1-MMP exocytosis in cancer invasion. *J. Cell Biol.* **211**, 339-358.

Maxfield, F. R. and McGraw, T. E. (2004). Endocytic recycling. *Nat. Rev. Mol. Cell Biol.* **5**, 121-132.

Monier, S., Chardin, P., Robineau, S. and Goud, B. (1998). Overexpression of the ARF1 exchange factor ARNO inhibits the early secretory pathway and causes the disassembly of the Golgi complex. *J. Cell Sci.* **111**, 3427-3436.

Montesinos, M. L., Castellano-Muñoz, M., García-Junco-Clemente, P. and Fernández-Chacón, R. (2005). Recycling and EH domain proteins at the synapse. *Brain Res. Brain Res. Rev.* **49**, 416-428.

Morad, S. A. F. and Cabot, M. C. (2013). Ceramide-orchestrated signalling in cancer cells. *Nat. Rev. Cancer* **13**, 51-65.

Morishige, M., Hashimoto, S., Ogawa, E., Toda, Y., Kotani, H., Hirose, M., Wei, S., Hashimoto, A., Yamada, A., Yano, H. et al. (2008). GEP100 links epidermal growth factor receptor signalling to Arf6 activation to induce breast cancer invasion. *Nat. Cell Biol.* **10**, 85-92.

Muralidharan-Chari, V., Hoover, H., Clancy, J., Schweitzer, J., Suckow, M. A., Schroeder, V., Castellino, F. J., Schorey, J. S. and D'Souza-Schorey, C. (2009a). ADP-ribosylation factor 6 regulates tumorigenic and invasive properties in vivo. *Cancer Res.* **69**, 2201-2209.

Muralidharan-Chari, V., Clancy, J., Plou, C., Romao, M., Chavrier, P., Raposo, G. and D'Souza-Schorey, C. (2009b). ARF6-regulated shedding of tumor cell-derived plasma membrane microvesicles. *Curr. Biol.* **19**, 1875-1885.

Ogretmen, B. and Hannun, Y. A. (2001). Updates on functions of ceramide in chemotherapy-induced cell death and in multidrug resistance. *Drug Resist. Update* **4**, 368-377.

Ogretmen, B. and Hannun, Y. A. (2004). Biologically active sphingolipids in cancer pathogenesis and treatment. *Nat. Rev. Cancer* **4**, 604-616.

Olivera-Couto, A., Graña, M., Harispe, L. and Aguilar, P. S. (2011). The eisosome core is composed of BAR domain proteins. *Mol. Biol. Cell* **22**, 2360-2372.

Pan, T., Sun, J., Hu, J., Hu, Y., Zhou, J., Chen, Z., Xu, D., Xu, W., Zheng, S. and Zhang, S. (2014). Cytohesins/ARNO: the function in colorectal cancer cells. *PLoS ONE* **9**, e90997.

Parachoniak, C. A., Luo, Y., Abella, J. V., Keen, J. H. and Park, M. (2011). GGA3 functions as a switch to promote Met receptor recycling, essential for sustained ERK and cell migration. *Dev. Cell* **20**, 751-763.

Paz, H., Pathak, N. and Yang, J. (2014). Invading one step at a time: the role of invadopodia in tumor metastasis. *Oncogene* **33**, 4193-4202.

Perryman, M. S., Tessier, J., Wiher, T., O'Donoghue, H., McCracken, A. N., Kim, S. M., Nguyen, D. G., Simitian, G. S., Viana, M., Rafelski, S. et al. (2016). Effects of stereochemistry, saturation, and hydrocarbon chain length on the ability of synthetic constrained azacyclic sphingolipids to trigger nutrient transporter down-regulation, vacuolation, and cell death. *Bioorg. Med. Chem.* **24**, 4390-4397.

Prescott, A. R., Lucocq, J. M., James, J., Lister, J. M. and Ponnambalam, S. (1997). Distinct compartmentalization of TGN46 and beta 1,4-galactosyltransferase in HeLa cells. *Eur. J. Cell Biol.* **72**, 238-246.

Rahajeng, J., Giridharan, S. S. P., Cai, B., Naslavsky, N. and Caplan, S. (2012). MICAL-L1 is a tubular endosomal membrane hub that connects Rab35 and Arf6 with Rab8a. *Traffic* **13**, 82-93.

Reinecke, J. B., Katafiasz, D., Naslavsky, N. and Caplan, S. (2015). Novel functions for the endocytic regulatory proteins MICAL-L1 and EHD1 in mitosis. *Traffic* **16**, 48-67.

Romero Rosales, K., Singh, G., Wu, K., Chen, J., Janes, M. R., Lilly, M. B., Peralta, E. R., Siskind, L. J., Bennett, M. J., Fruman, D. A. et al. (2011). Sphingolipid-based drugs selectively kill cancer cells by down-regulating nutrient transporter proteins. *Biochem. J.* **439**, 299-311.

Sangodkar, J., Farrington, C. C., McClinch, K., Galsky, M. D., Kastrinsky, D. B. and Narla, G. (2016). All roads lead to PP2A: exploiting the therapeutic potential of this phosphatase. *FEBS J.* **283**, 1004-1024.

Santy, L. C. (2002). Characterization of a fast cycling ADP-ribosylation factor 6 mutant. *J. Biol. Chem.* **277**, 40185-40188.

Santy, L. C. and Casanova, J. E. (2001). Activation of ARF6 by ARNO stimulates epithelial cell migration through downstream activation of both Rac1 and phospholipase D. *J. Cell Biol.* **154**, 599-610.

Schweitzer, J. K., Sedgwick, A. E. and D'Souza-Schorey, C. (2011). ARF6-mediated endocytic recycling impacts cell movement, cell division and lipid homeostasis. *Semin. Cell Dev. Biol.* **22**, 39-47.

Selwan, E. M., Finicle, B. T., Kim, S. M. and Edinger, A. L. (2016). Attacking the supply wagons to starve cancer cells to death. *FEBS Lett.* **590**, 885-907.

Sharma, M., Giridharan, S. S. P., Rahajeng, J., Naslavsky, N. and Caplan, S. (2009). MICAL-L1 links EHD1 to tubular recycling endosomes and regulates receptor recycling. *Mol. Biol. Cell* **20**, 5181-5194.

Skrzypek, M. S., Nagiec, M. M., Lester, R. L. and Dickson, R. C. (1998). Inhibition of amino acid transport by sphingoid long chain bases in Saccharomyces cerevisiae. *J. Biol. Chem.* **273**, 2829-2834.

Sodek, K. L., Ringuette, M. J. and Brown, T. J. (2007). MT1-MMP is the critical determinant of matrix degradation and invasion by ovarian cancer cells. *Br. J. Cancer* **97**, 358-367.

Summers, S. A., Garza, L. A., Zhou, H. and Birnbaum, M. J. (1998). Regulation of insulin-stimulated glucose transporter GLUT4 translocation and Akt kinase activity by ceramide. *Mol. Cell. Biol.* **18**, 5457-5464.

Swingle, M., Ni, L. and Honkanen, R. E. (2007). Small-molecule inhibitors of ser/thr protein phosphatases: specificity, use and common forms of abuse. *Methods Mol. Biol.* **365**, 23-38.

Tague, S. E., Muralidharan, V. and D'Souza-Schorey, C. (2004). ADP-ribosylation factor 6 regulates tumor cell invasion through the activation of the MEK/ERK signaling pathway. *Proc. Natl. Acad. Sci. USA* **101**, 9671-9676.

Trajkovic, K., Hsu, C., Chiantia, S., Rajendran, L., Wenzel, D., Wieland, F., Schwille, P., Brügger, B. and Simons, M. (2008). Ceramide triggers budding of exosome vesicles into multivesicular endosomes. *Science* **319**, 1244-1247.

Vidal-Quadras, M., Gelabert-Baldrich, M., Soriano-Castell, D., Lladó, A., Rentero, C., Calvo, M., Pol, A., Enrich, C. and Tebar, F. (2011). Rac1 and calmodulin interactions modulate dynamics of ARF6-dependent endocytosis. *Traffic* **12**, 1879-1896.

Walseng, E., Bakke, O. and Roche, P. A. (2008). Major histocompatibility complex class II-peptide complexes internalize using a clathrin- and dynamin-independent endocytosis pathway. *J. Biol. Chem.* **283**, 14717-14727.

Walther, T. C., Brickner, J. H., Aguilar, P. S., Bernales, S., Pantoja, C. and Walter, P. (2006). Eisosomes mark static sites of endocytosis. *Nature* **439**, 998-1003.

Welsch, C. A., Roth, L. W. A., Goetschy, J. F. and Movva, N. R. (2004). Genetic, biochemical, and transcriptional responses of Saccharomyces cerevisiae to the novel immunomodulator FTY720 largely mimic those of the natural sphingolipid phytosphingosine. *J. Biol. Chem.* **279**, 36720-36731.

Yoo, J. H., Shi, D. S., Grossmann, A. H., Sorensen, L. K., Tong, Z. Z., Mleynek, T. M., Rogers, A., Zhu, W., Richards, J. R., Winter, J. M. et al. (2016). ARF6 is an actionable node that orchestrates oncogenic GNAQ signaling in Uveal melanoma. *Cancer Cell* **29**, 889-904.

Zhao, H., Ahirwar, D. K., Oghumu, S., Wilkie, T., Powell, C. A., Nasser, M. W., Satoskar, A. R., Li, D. Y. and Ganju, R. K. (2016). Endothelial Robo4 suppresses breast cancer growth and metastasis through regulation of tumor angiogenesis. *Mol. Oncol.* **10**, 272-281.

Zimmermann, P., Zhang, Z., Degeest, G., Mortier, E., Leenaerts, I., Coomans, C., Schulz, J., N'Kuli, F., Courtoy, P. J. and David, G. (2005). Syndecan recycling [corrected] is controlled by syntenin-PIP2 interaction and Arf6. *Dev. Cell* **9**, 377-388.